

# Comparative Study of Asymmetry Origin of Galaxies in Different Environments. I. Optical observations.

I. Plauchu-Frayn<sup>1</sup> & R. Coziol<sup>1</sup>

plauchuf@astro.ugto.mx, rcoziol@astro.ugto.mx

## ABSTRACT

This paper presents the first of two analyses about the influence of environment on the formation and evolution of galaxies observed in the nearby universe. For our study, we used three different samples representing different density environments: galaxies in Compact Groups (HCGs), Isolated Pairs of Galaxies (KPGs), and Isolated Galaxies (KIGs), which were taken as references. Using both characteristic isophotal parameters and evidence of asymmetries in the optical and the near-infrared, we are able to establish differences in the characteristics of galaxies with different morphologies in different environments, allowing us to better understand their different formation histories. In this first paper we present the isophotal and asymmetry analyses of a sample of 214 galaxies in different environments observed in the optical ( $V$  and  $I$  images). For each galaxy, we have determined different characteristic isophotal parameters and  $V - I$  color profiles, as a function of semi-major axis, and performed a full asymmetry analysis in residual images using the  $V$  filter. Evidence of asymmetry in the optical is almost missing in the KIG sample, and significantly more common in the KPG than in the HCG samples. Our isophotal analysis suggests that the stellar populations in the HCG galaxies are older and more dynamically relaxed than in the KPG. The HCG galaxies seem to be at a more advanced stage of interaction than the KPGs. One possible explanation is that these structures formed at different epochs: compact groups of galaxies would have formed before close pairs of galaxies, which only began interacting recently. However, similarities in the formation process of galaxies with same morphology suggest CGs and close pairs of galaxies share similar conditions; they are new structures forming relatively late in low-density environments.

*Subject headings:* galaxies: interactions – galaxies: photometry – galaxies: structure

## 1. Introduction

Although it is recognized that the environment of galaxies plays an important role in their formation and evolution, the mechanisms responsible for such processes, the details on how they apply, and the time-scales on which they are effective are still largely unknown. For example, in Compact Groups of Galaxies (CGs) we have recently shown (Coziol & Plauchu-Frayn 2007) that mergers and tidal interactions are two important mechanisms driving the morphological evolution of galaxies in

these systems. We have also found that many of the ongoing merger events were possibly happening without gas, a phenomenon known in the literature as a “dry merger” (van Dokkum 2005). According to the dry merger hypothesis, elliptical galaxies are generally formed by the merger of bulge-dominated galaxies, not from the merger of spiral-like galaxies. This is fully consistent with the CG environment where early-type galaxies constitute the dominant population (Coziol et al. 2004). Finding evidence of dry mergers in CGs is important, because it suggests that these systems are obviously not in a dynamically stable state. It also suggests that since the merging process of the galaxies is not yet complete, these systems cannot

---

<sup>1</sup>Departamento de Astronomía, Universidad de Guanajuato Apartado Postal 144, 36000 Guanajuato, Gto, México

be as old as that believed based on the absence of standard observational merging evidence, like luminous active galactic nuclei (AGNs), recent star formation events, or post-burst stellar populations in evolved galaxies.

What is missing in CGs is a time scale for the evolution process of the galaxies. Was the evolution of galaxies accelerated in the group environment? Is the dry merger the result of such evolution? Is the dry merger limited only to dense environments? What is the role of the potential of the group in the disappearance of the gas? How fast was the gas exhausted or consumed? Did it burn rapidly forming the bulges of numerous early-type galaxies, was it lost feeding a black hole, or was it mostly ripped off of the galaxies and lost to the intergalactic medium?

In order to find some answers to the above questions, we have decided important to extend our study of characteristic isophotal parameters and asymmetry to two different structures having lower spatial density than CGs: isolated galaxies and isolated pairs of galaxies. Isolated galaxies are considered to have a low probability of interaction with another galaxy of similar mass over a Hubble time (Vettolani, de Souza & Chincarini 1986). Consequently, a sample of isolated galaxies can be treated as a set of “comparison objects”, free during most of their lifetime from environmental effects. Isolated galaxies are uncommon in the universe where most of the galaxies tend to be clustered in groups, as shown by Tully (1987). The reason for their existence, therefore, may be an interesting subject of study by itself. Isolated pairs of galaxies are in the next level of galaxy density. In the nearby universe, these systems are also rare and consequently their history is not well documented. Many questions still need to be answered. How long have these galaxies been interacting? Are they engaged in first encounters or did they interact multiple times before with their companions? Are these transient phenomena (high-energy orbits) or merging encounters (low-energy or decaying orbits)?

For our study, we used three well-defined environment samples: the Catalog of Isolated Galaxies (KIGs), from Karachentseva (1973), the list of Isolated Pairs of Galaxies (KPGs), as compiled by Karachentsev (1972), and the Catalog of Compact Groups of Galaxies (HCGs) from Hick-

son (1982). Our analysis is based on the application of two independent methods: the fitting of elliptical ellipses on the isophotal levels of the galaxies and the determination of their asymmetry (Coziol & Plauchu-Frayn 2007). We present the characteristics of the observed samples in Section 2 and describe our observations and the reduction process in Section 3. In Section 4, we explain the methods used for our analysis. The surface photometry profiles, the color maps and asymmetrical images of the observed galaxies, and the results of nonparametric statistical tests used to establish the level of significance of the differences observed are presented in Section 5. Finally, we discuss our results and give our conclusions in Section 6. Our analysis for the near-infrared will follow in an accompanying paper (Plauchu-Frayn & Coziol 2010).

## 2. Selection and properties of the observed galaxies

### 2.1. Isolated Galaxies

In 1973, Karachentseva used a simple method for identifying isolated galaxies. By inspecting the blue prints of the Palomar Observatory Sky Survey (POSS) she selected all the galaxies in the Zwicky catalog (Zwicky et al. 1961-1968) whose nearest neighbor has a size within a factor 4 of the major-axis diameter of the target galaxy and lies more than 20 diameters away from it. This definition implies that a galaxy with a diameter of 20 kpc and peculiar velocity on the order of 150 km s<sup>-1</sup> has not been influenced by a similar mass galaxy during the last  $\sim 3$  Gyr (Turner et al. 1979). The KIGs are observed in the nearby universe ( $z < 0.14$  with median  $z = 0.02$ ) and have apparent magnitudes brighter than 15.7, which is the limit of the Zwicky catalog (Zwicky et al. 1961-1968). Members in this catalog have north declination  $\delta \geq -3^\circ$ , the majority being at high galactic latitudes ( $|b| \geq 20^\circ$ ).

### 2.2. Isolated pairs of galaxies

In the early 1970s, Karachentsev (1972) compiled what was at that time the first list of pairs of galaxies, the Catalog of Isolated Pairs of Galaxies (KPGs). Using the Zwicky catalog, the KPGs were selected from visual inspection of the POSS prints based solely on their observed properties,

like apparent separation, apparent magnitudes, and angular diameters, and without reference to apparent signs of interaction. The pairs of galaxies in the KPG are also located in the nearby universe ( $z < 0.06$  with median  $z = 0.02$ ), all have north declination  $\geq -3^\circ$ , high galactic latitude ( $|b| \geq 20^\circ$ ), and photographic magnitudes brighter than 15.7. This catalog is considered suitable for studying galaxies in pairs because of its size, completeness, and relatively unbiased selection (Hernández-Toledo et al. 1999).

Subsequent spectroscopic observations revealed that only half of the KPGs in the initial catalog have small relative velocities,  $\Delta v < 100 \text{ km s}^{-1}$ , while the remaining pairs have relative velocities extending upward and as far as  $10,000 \text{ s}^{-1}$  (Karachentsev 1987). Later on various attempts to establish solid criteria to determine true pairs based on the relative velocity of the member galaxies were made. For example, Turner (1976) proposed that physical pairs must have  $\Delta v < 425 \text{ km s}^{-1}$ . According to Makino & Hut (1997), pairs of galaxies have a higher probability to show effects due to interaction when the difference in radial velocity between the two galaxies is comparable or lower than their internal velocity dispersion. In the same vein, Patton et al. (2000) suggested  $\Delta v \leq 500 \text{ km s}^{-1}$ . For our sample we have followed the latter authors and selected pairs with  $\Delta v \leq 500 \text{ km s}^{-1}$ .

In Figure 1, we show the linear separation and difference in radial velocity between the members of the KPG pairs. The majority are close pairs of galaxies, with spatial separation lower than 50 kpc and difference in radial velocity lower than or equal to  $150 \text{ km s}^{-1}$ . For comparison, our Local Group of galaxies as viewed at a comparable redshift ( $z \sim 0.02$ ) would look like a pair with a spatial separation of 772 kpc (Ribas et al. 2005) and a difference in radial velocity equal to  $112 \text{ km s}^{-1}$ . Therefore, the galaxies in the KPG are much closer than the two major galaxies in our Local Group.

### 2.3. Compact Groups of Galaxies

In the early 1980s, Paul Hickson conducted a visual search for CGs using red POSS prints in order to obtain a homogeneous sample that could be subjected to statistical analysis. Hickson's Compact Groups Catalog forms one of the most

studied samples to date (Hickson 1982). The HCGs are small systems of three to eight galaxies in apparent close proximity in the sky. The space density of galaxies is very high, often exceeding that of the cores of large clusters of galaxies (Hickson et al. 1992). The relatively low velocity dispersions, which are generally comparable to galaxy rotation velocities, make interactions and mergers common in these systems (Hickson et al. 1992). Many galaxies in the HCG show morphological peculiarities indicative of gravitational interactions (Mendes de Oliveira & Hickson 1994; Coziol & Plauchu-Frayn 2007).

In 1992, Hickson et al. (1992) obtained spectroscopic observations for almost all the galaxies in the HCG (462 galaxies) and found that only 92 groups are real bounded systems with at least three members and with a median radial velocity dispersion of  $200 \text{ km s}^{-1}$ . The HCGs are nearby universe structures (with  $z < 0.14$  and median redshift  $z = 0.03$ ), which are located well beyond the Virgo Cluster (Hickson et al. 1992). For our study, we have selected groups from Hickson et al. (1992) with velocity dispersions  $\sigma_v \leq 800 \text{ km s}^{-1}$ .

### 2.4. Observed samples

In Figure 2, we show the distribution of absolute  $B$  magnitude versus the virgocentric velocity for 308 HCG galaxies (top), 938 KPG galaxies (middle), and 777 KIG galaxies (bottom). Only galaxies inside the range  $900 \text{ km s}^{-1} \leq v_{vir} \leq 13,000 \text{ km s}^{-1}$ , with  $M_B \leq -15$ , and satisfying the previous selection criteria, are plotted in this figure. One can see that the KPG and KIG surveys scan comparable volumes. The HCG survey, on the other hand, being slightly deeper, contains galaxies with lower luminosity ( $M_B \leq -18$ ) above  $v_{vir} = 8000 \text{ km s}^{-1}$ . This difference will be taken into account during our analysis.

Based on the samples we set up our targets on galaxies with declinations in the range  $-32^\circ \leq \delta \leq +55^\circ$  and the semi-major axis in the range  $0'.5 \leq a \leq 3'.5$ , which allows for optimal spatial resolution. Also, to minimize inclination corrections for photometric data to evaluate of basic structural parameters, we have applied an ultimate criterion based on the semi-minor to semi-major axis ratio, keeping galaxies with  $b/a \geq 0.4$  (or  $i \leq 70^\circ$ ). Only in a few cases, in the HCG, applying this last criterion was impossible.

Our final selection for the observed galaxies also depended on the time allocated for observation and the weather conditions. We were able to observe in total 214 galaxies: 37 KIGs, 71 KPGs, and 106 HCGs. All the galaxies have redshifts  $z < 0.04$ . The properties of these galaxies are reported in Tables 1-tabl3. For each of the galaxies, we have double checked the morphological type. Most of the KIG galaxies already had their morphology determined by Sulentic et al. (2006). In the cases where our CCD images and isophotal study suggested a bar, we have added this information to their morphological description.

In Figure 3, we compare the characteristics of the observed samples with the characteristics of the galaxies in their respective catalogs. One can see that the observed samples reproduce the absolute and morphological distribution of their parent samples relatively well. The results of non-parametric statistical tests (Mann-Whitney), presented in Table 4, are consistent with no differences in absolute magnitude and size, although there seems a slight tendency for the observed KIGs to be nearer than the galaxies in their parent sample.

### 3. Observation and reduction

The sample of 214 galaxies was imaged during five different observing missions (see Table 5). The observations were carried out using the 1.5 m telescope of the Observatorio Astronómico Nacional, located at the Sierra San Pedro Mártir in Baja California, México. Depending on the observing run, there were two different detectors attached to the telescope (see Table 5): the Site1 and the Marconi CCDs. The first CCD covers an area of about  $4.3' \times 4.3'$  on the sky, with a spatial resolution of  $0.26''$  per pixel. The second one covers an area about  $4.5' \times 4.5'$  with a spatial resolution of  $0.28''$  per pixel, using a  $2 \times 2$  binning mode. For each galaxy we took three images in each filter, with exposure times of 600-900 s in  $V$  and 200-300 s in  $I$ . Each night standard stars were also observed to calibrate the data in flux. These stars were taken from the Landolt Equatorial Stars list (Landolt 1992) and cover a wide range in color:  $-0.30 \leq (V - I) \leq 2.63$  or  $-1.12 \leq (B - V) \leq 2.33$ .

The nights were clear during the last four observing runs, with average effective seeing condi-

tions at the telescope of  $1.6''$ ,  $1.9''$ ,  $1.8''$ , and  $1.4''$ , respectively. During the first run, all nights were not totally clear, with an average effective seeing of  $2.4''$ . During this run, we used a binning mode of  $2 \times 2$  with the Site1 CCD to increase the signal-to-noise (S/N). Note that because the surface brightness, ellipticity, position angle (P.A.), and asymmetry profiles depend only on the S/N and spatial resolution in a frame, a high photometry accuracy is not important for our analysis.

The data were reduced and calibrated using standard algorithms in IRAF<sup>1</sup>. The images were first trimmed in order to remove bad lines and columns at the edges from the CCD and to reduce vignetting effects. We subsequently applied a mask on all the images to remove the bad pixels on the CCD. An average bias (combining 15-20 bias images) was subtracted from the object images and the flat frames. Several sky flat frames taken in each filter at the beginning and/or end of each night were normalized, combined, and then divided from each object image. The level of unflattening is well below 2%, and the flat fielding conserves the flux to better than 99%. Cosmic-ray removing was done using the *COSMICRAYS* task. Resilient cosmic rays were corrected by hand using the *IMEDIT* task. To each image, a small shift (a tenth of a pixel) was applied to correct telescope drifting or repositioning. After trimming the images to the same dimension, they were averaged together. The final reduction step consisted of eliminating the sky contribution. This was done by measuring the mean flux within  $5 \times 5$  pixel boxes all around the targets (where there are no stars or background objects) and subtracting this value from the images.

The instrumental magnitudes were estimated by measuring the flux of each observed standard star. Air-mass correction was applied using extinction coefficients proper to San Pedro Mártir (Schuster & Parrao 2001). The calibration equations were determined by fitting linear regressions on the observed values. For photometric errors, we adopt the standard deviation between our estimated magnitude and the magnitude de-

<sup>1</sup> IRAF is the Image Analysis and Reduction Facility made available to the astronomical community by the National Optical Astronomy Observatory, which is operated by AURA, Inc., under contract with the U.S. National Science Foundation.

terminated by Landolt (1992). Magnitudes for the observed galaxies have also been corrected for galactic extinction (Schlegel, Finkbeiner & Davis 1998). Due to the low redshifts of the galaxies (median  $z = 0.02$ ) no  $K$ -correction was applied, since these are smaller (e.g., 0.02 in  $V - I$ ) than our uncertainties. The general characteristics of the observations are given in Table 5.

Note that the calibration in flux was done after the different analysis (ellipse fitting and asymmetry) were performed. This method avoids keeping the noise in the images at low level producing the highest possible S/N.

#### 4. Description of the analysis methods

Three analyses were performed on each galaxy: fitting of ellipses, formation of color maps, and estimation of asymmetry level. Here we describe the methods used and information obtained from each analysis.

Our analyses in different bands (optical and near-infrared, (NIR)) yield information over different time-scales. In the optical, our analysis is sensible to young or intermediate age stellar populations and dust extinction. In the NIR, our analysis is sensible to older stellar populations, and consequently to mass distributions (Coziol & Plauchu-Frayn 2007; Plauchu-Frayn & Coziol 2010).

##### 4.1. Isophotal method analysis and color maps

Surface photometry was carried out on each galaxy. This was done within STSDAS<sup>2</sup> with the ELLIPSE task (Jedrzejewski 1987). The algorithm used by this task derives various geometric parameters, such as surface brightness  $\mu$ , ellipticity  $\epsilon$ , P.A., and the harmonic amplitude  $B_4$ . This last parameter is related to the standard fourth-order Fourier cosine coefficient,  $a_4$  (Bender, Döbereiner & Möllenhoff 1988), normalized to the semi-major axis  $a$  at which the ellipse was fitted ( $a_4/a = B_4\sqrt{1-\epsilon}$ ). Another important parameter is the  $V - I$  color index profile. This profile is obtained by measuring the  $V$

and  $I$  magnitude profiles, subtracting one from the other.

The only requirement for ELLIPSE to work is an initial guess of the geometric center,  $\epsilon$ , and of P.A., of the galaxy. The geometrical center of a galaxy is determined by locating the peak in light distribution (Coziol & Plauchu-Frayn 2007). The default  $\epsilon$  and P.A. were 0.05 and 0, respectively. The task ELLIPSE is applied keeping the geometric center fixed and allowing  $\epsilon$  and P.A. to vary. This method yields surface brightness and color profiles that match the local variations of the structural components. We also restrict the fit of ellipses in the central part of the galaxy to a radius larger than the seeing (see Figure 4) and minimize the light contribution from companion galaxies (important only for the HCGs and KPGs) by stopping the task manually at the maximum radius possible.

The isophotal parameters measured by ELLIPSE provide important information on the physical morphology and are intimately related to the dynamical properties of the galaxies (Barth Coziol & Demers 1995; Coziol & Plauchu-Frayn 2007). For example, large variations in P.A.  $\sim 20^\circ$ , or twists (Nieto et al. 1992), usually reflect inhomogeneous mass distributions (Zaritsky & Lo 1986), while  $\epsilon$  variations reflect bars, dust, mass perturbations, or small disks in the central regions of early-type galaxies. Early isophotal studies have shown that large isophotal twists are only measured in interacting galaxies, suggesting that they are the consequence of close encounters or mergers (Kormendy 1982; Bender & Möllenhoff 1987). In our analysis we define a twist,  $\theta$ , as a variation in P.A. accompanied by a monotonically varying ellipticity  $\epsilon$  with amplitude  $\Delta\epsilon \geq 0.1$ . This definition allows differentiating between variations of P.A. produced by triaxiality and from those produced by interactions (Kormendy 1982; Bender & Möllenhoff 1987).

The isophotal deviations from the pure ellipse, quantified by the  $a_4$  coefficient, determine the characteristic shape of the isophote: boxy ( $a_4 < 0$ ), consistent with a pure elliptical or round isophote ( $a_4 \sim 0$ ), or disk ( $a_4 > 0$ ), consistent with a slightly pointed isophote. Elliptical galaxies with disk isophotes tend to be faint. They generally contain a rapidly rotating stellar population with a nearly isotropic velocity dispersion.

<sup>2</sup>STSDAS is distributed by the Space Telescope Science Institute, which is operated by the Association of Universities for Research in Astronomy (AURA), Inc., under NASA contract NAS 5-26555

Elliptical galaxies with boxy isophotes tend to be luminous and massive. They have anisotropic velocity dispersion and are thought to be supported by pressure rather than stellar rotation. These differences suggest two distinct formation scenarios for boxy and disk elliptical galaxies. Numerical simulations have shown that the formation processes depend highly on the initial conditions: initial mass ratios, individual angular momentum, dust and gas contents of the merging galaxies (Hernquist 1993; Barnes 1996). The general idea is that mergers between unequal-mass, gas-rich galaxies tend to produce disk early-type remnants, while mergers with equal-mass, high-density, and gas-poor galaxies tend to produce boxy remnants (Naab & Burkert 2003).

The concentration index,  $C$ , is a measure of the light concentration of a galaxy profile, having high values for centrally concentrated light profiles. It is well known that the concentration index has a tight correlation with morphological type (Abraham et al. 1994; Shimasaku et al. 2001); early-type galaxies tend to have the most concentrated light profiles, while late-type galaxies have the least concentrated ones. Interactions between galaxies can also perturb the stellar material, changing the light profiles of the galaxies in the process and affecting their concentration index.

Because we are studying nearby galaxies, the spatial resolution of our CCD images allows us to measure the  $C$  parameter at different radii. Based on the isophotal profiles of the galaxies, we have estimated  $C$  values inside and outside a physical radius  $r_0$ , independent of the distribution of light. To estimate this radius, we have used the major axis at 25 mag arcsec<sup>-2</sup> (Paturel et al. 2003) as given in Hyperleda and determined the linear diameters in  $B$  magnitude,  $D_B$ , for the galaxies in the HCG, KPG, and KIG catalogs estimating the median of the three distributions. The median value obtained is 23 kpc. In our sample, a few galaxies (20% of the sample: 26 HCGs, 12 KPGs, and 4 KIGs) turned out to have a  $D_B$  that is smaller than this value. Consequently, we have used two different  $r_0$ ; one is equal to 5 kpc (approximately  $D_B/4$ ) for the standard size galaxies (approximately  $M_V < -20$ ) and the other is half of this value, 2.5 kpc, for galaxies with smaller diameters. For our analysis we give three concentra-

tion indices: one inside  $r_0$ ,  $C(r < r_0) = \mu(r = r_0) - \mu(r < r_0)$ , one outside  $r_0$ ,  $C(r > r_0) = \mu(r > r_0) - \mu(r = r_0)$  and a global (or total) concentration index  $C_{Total} = \mu(r > r_0) - \mu(r < r_0)$ .

For the sake of comparison, in our analysis we have also chosen a radius which depends on the light distribution in the galaxies. We have used the Petrosian,  $R_P$ , and effective radii,  $R_e$ , as determined based on a modified form of the Petrosian (1976) system (Graham et al. 2005). In this system  $R_P$  is defined as the projected radius where  $1/\eta(R_P) = 0.2$ . The Petrosian index,  $\eta(R) = \langle I \rangle_R / I(R)$ , is the ratio of the intensity of an isophote at radius  $R$  and the average intensity within that radius, as measured using circular apertures. In the case of small galaxies, where the faint central surface brightness does not allow us to reach  $1/\eta(R_P) = 0.2$ , we have used  $1/\eta(R_P) = 0.4$  instead. In Tables 6 and 7, for all the galaxies in our analysis we give  $R_P$ ,  $R_e$ , the magnitude inside the effective radius;  $M_e$ , a concentration index, which is defined as the ratio of radii that contain 90% and 50% of the Petrosian flux,  $R_{90\%}/R_{50\%}$ ; the surface brightness at the effective radius,  $\mu_e$ ; and the color at this radius.

Finally, as a complementary analysis, we have constructed a  $V - I$  color map for each observed galaxy. We present these maps in the bottom right part of Figure 4. In these maps, bright regions are consistent with red stellar population or dust extinction, and dark regions are consistent with blue stellar populations. These color distribution maps were found to be extremely useful in detecting tidal tails, galaxy satellites, dusty patches, and common envelopes in galaxies.

## 4.2. Asymmetry method analysis

Another useful method for the study of morphology consists of estimating the level of asymmetry of a galaxy (Abraham et al. 1994, 1996; Schade et al. 1995; Conselice 1997, 2000; Coziol & Plauchu-Frayn 2007; Hutchings & Proulx 2008). The leitmotif behind this method is that the level of asymmetry of a galaxy reflects something about its history of formation and evolution. For example, galaxies that are old and already well evolved, or galaxies that formed in isolation, are expected to possess fairly symmetric distributions of light. On the other hand, galaxies affected by interactions or mergers sometime during their evolution are ex-

pected to show more complex distributions.

The interpretation of asymmetry may seem straightforward enough for early-type galaxies, but it is not that simple for later-type spiral galaxies. Various studies have shown that in late-type spirals, asymmetric structures may result from intrinsic processes related to star formation (Schade et al. 1995; Conselice 2000). Extra care must be taken, therefore, before drawing conclusions about the origin of asymmetries in any sample of galaxies. In Coziol & Plauchu-Frayn (2007) it was shown that the asymmetric structure analysis is complementary to the isophotal one: there is a one-to-one relation between the variations of isophotal characteristic parameters and the existence of asymmetries related to inhomogeneous distribution of mass produced by interaction effects. Applying the two analyses in parallel yields a high confidence level when interpreting the results.

For the present analysis we have used a slightly different measure of asymmetry than that found in the literature (also different from the one used in Coziol & Plauchu-Frayn 2007). This was done in order to make the interpretation more straightforward. The principle of the asymmetry method is relatively simple (see Coziol & Plauchu-Frayn 2007 for details). The image of a galaxy is rotated by  $180^\circ$  and divided from the original image. Any differences in the distribution of light (asymmetries) appear under the form of excesses of light (bright regions), together with their corresponding shadows (dark regions) on the opposite side (see Figure 4).

To measure the asymmetry level, the residual images are smoothed using boxes of size equal to the seeing in pixels, reducing the noise. Ellipses are then fitted to the residual image of each galaxy, keeping the center, ellipticity, and P.A. fixed. The level of asymmetry as a function of semi-major axis  $a$  is estimated by the following formula:

$$A(a)_{180^\circ} \equiv \frac{I_0}{I_{180^\circ}} \quad (1)$$

where  $I(a)_0$  is the intensity in the original image and  $I(a)_{180}$  is the intensity in the rotated image. This formula yields values between 1 (completely symmetric) and  $> 1$  (completely asymmetric).

Comparing with the residual images ( $I_0/I_{180}$ ) it is easy to verify that asymmetries in our analysis appear as structures in the asymmetry curve. The amplitudes of these structures are proportional to their relative intensities. For example, an asymmetry of  $A = 1.2$  indicates a concentration of light 20% brighter than the intensity at that radius on the opposite side. This corresponds to a high level of asymmetry. On the other hand, a level of asymmetry of  $A = 1.0$  indicates that the intensity of light is the same on both sides (complete symmetry). In our analysis, a symmetric distribution of light yields a flat asymmetry curve (see the bottom left graphic in Figure 4).

For our asymmetry analysis determining the center of the galaxies around which the rotation is done is a crucial step. If this is not done carefully spurious asymmetries can be produced. The method we used (finding the peak in luminosity; see Coziol & Plauchu-Frayn 2007) is simple and yields excellent results. It has also the advantage to correspond to the same center as used during the isophotal analysis. As a check, one can verify that, as expected, at the center of the galaxies the asymmetry curves have a level of 1 (minimum asymmetry). Moreover, real asymmetries produce isophotal structures that are detected by our first analysis based on ellipses fitting. Therefore, we are secure that no spurious asymmetries are produced by our method.

Our analysis is not sensitive to sky gradients, because it applies to the inner part of the galaxies, minimizing the possible contamination by foreground stars. When needed, foreground stars were eliminated using masks (using IMEDIT in IRAF). When a star was found lying very near the body of a galaxy, a special mask was used within ELLIPSE itself. In cases where it was impossible to eliminate the contaminating star the galaxy was rejected.

## 5. Results of analysis

In Figure 4, we show the mosaic for one very symmetric galaxy (the full sample of mosaic images is available in the online version of the journal). On the left of the figure, we present the isophotal profiles, where the dashed vertical line indicates an average half-radius of  $r_0 = 5$  kpc (or  $r_0 = 2.5$  kpc, as used for small size galax-

ies). On the right, we present the  $V$ -band image, displayed on a logarithmic scale with superimposed isophotes. We also present the residual image from the asymmetry analysis (middle right) and the  $V - I$  color map (bottom image). In all these images, the north is at the top and east is to the left.

In Coziol and Plauchu-Frayn (2007) we have shown that the isophotal and asymmetry analysis are consistent, yielding complementary information. We will not repeat this analysis here, but give only two examples. In Figure 5(a), we show the asymmetrical galaxy HCG 93b. The level of asymmetry increases by 20% at a radius of 18 arc-sec. This asymmetry is accompanied by a sudden significant variation in the three isophotal parameters. In the case of the symmetric galaxy KPG 539A, Figure 5(b), the absence of asymmetries is accompanied by a smooth variation in the isophotal parameters.

### 5.1. Comparison of galaxies with same morphologies in different environments

For our analysis, we have divided our samples into three morphology groups: early type (E–S0), intermediate type (Sa–Sb), and late types (Sbc–Im). The median characteristics of the galaxies in these three different groups are reported in Tables 8–10 for properties measured at radius  $r_0$  and in Tables 11–13 for properties measured at radius  $R_e$ . We now discuss the variations of the various characteristics encountered in each group depending on their environments. To check for the statistical significance of the variations observed, nonparametrical tests (Kruskal–Wallis or Mann–Whitney and Dunn’s post-tests) were also performed. All the tests were done at a level of significance of 95%, which is the standard for these kinds of tests. Description of the tests used can be found in Coziol (2003). The results of the statistical tests are reported in the last columns of Tables 8–10 and Tables 11–13.

#### 5.1.1. Early-type (E–S0) galaxies

In Figures 6 and 7, we show the variations of the isophotal parameters in early-type galaxies internal to  $r_0$  (Figure 6) and external to  $r_0$  (Figure 7). In each graph, the  $x$ -axis represents the absolute

magnitude in  $V$ , as estimated inside  $r_0$ .

In this morphology group, there are only three galaxies that belong to the KIGs. We have discarded these from our statistical tests. The KPG galaxies in this morphology group tend to be slightly bluer than the HCG, and this is independent of the radius and absolute magnitude of the galaxies. This is confirmed by our statistical tests (see Tables 8 and 9 for  $r_0$  and  $R_e$ , respectively). Inside the half-radius, the HCG galaxies tend to be less concentrated than the KPG galaxies. This is also confirmed by our statistical tests (see Table 8).

The higher concentration and bluer color observed for the E–S0 KPG galaxies are consistent with the idea of recent gas accretion and an increase of star formation in the center of these galaxies. Outside the half-radius, there are no differences in concentration between the KPGs and the HCGs. This also agrees with the absence of difference based on  $R_{90\%}/R_{50\%}$ , since this parameter is estimated at comparable radii (Table 9).

There are no significative differences between the KPG and HCG galaxies in surface brightness inside the half-radius. Farther out the HCG galaxies tend to have slightly higher surface brightness than the KPGs (see Table 8). Since we are observing in the optical, this suggests older stellar populations or more relaxed structures as a whole in the HCGs, which is also consistent with the slightly redder colors for the HCG galaxies.

Due to the low value of  $R_e$  compared to  $r_0$ , the statistical tests find higher surface brightness on average for the early-type KPG galaxies as compared to the HCGs (see Table 9). This is consistent with our interpretation of more relaxed populations of stars in the HCGs than in the KPGs.

In terms of asymmetry, we do not find any significative differences among the samples. This morphological type appears to be very symmetric independent of the environment. This suggests similar formation mechanisms for these galaxies.

For early-type galaxies, we can verify what types of isophotes are prevailing: boxy with  $a_4 < 0$  or diskly with  $a_4 > 0$ . In Figure 8 we show the values of  $a_4$  as measured at the half-radius for the E–S0 galaxies in different environments. One can see that both the HCG and KPG E–S0 galaxies tend to occupy the region of diskly galaxies: 38 out

of 57 (67%) of the HCGs and 15 out of 25 (60%) for the KPGs. The ellipticity of these galaxies is also quite high. This is consistent with the hypothesis of similar mechanisms for the formation of these galaxies in both environments. For example, the transformation of later-type spirals through gas accretion and star formation in the central part would be one way to produce E–S0-like galaxies that have diskly rather than boxy isophotes.

Evidence in favor of similar mechanisms for the formation of E–S0 galaxies in the KPGs and HCGs can also be found in the high frequency of detection of isophotal twists in both samples: 40% (10/25) in the KPGs and 51% (29/57) in the HCGs. The levels of the twists in these galaxies are shown in Figure 9 as a function of absolute magnitude in  $V$ . We consider large twists to be those with values  $\theta > 20^\circ$ . The median values of  $\theta$  are  $25^\circ$  and  $20^\circ$  for the KPGs and HCGs, respectively.

In Figure 10, we show how the isophote parameter  $a_4$  and twist  $\theta$  vary with the ellipticity difference  $\Delta\epsilon = \epsilon_{max} - \epsilon_{min}$ . Values of  $\Delta\epsilon > 0$  indicate that the galaxies are generally rounder in their centers than in their periphery. Large values in  $\Delta\epsilon$  together with large  $|a_4| > 0.7$  and  $\theta > 20^\circ$  suggest the galaxies were possibly affected by interactions. No significant differences are observed between the HCGs and the KPGs, suggesting, once again, similar formation mechanisms.

In Figure 3, we show the distribution of the morphology of the galaxies in the different catalogs. We observe a clear increase in the number of earlier-type galaxies among the HCGs compared with the KPGs and KIGs. The fact that we found a higher number of S0 galaxies among the HCGs than among the KPGs suggests interactions and mergers are possible mechanisms responsible for forming these galaxies. At the same time, the fact that we also find S0 galaxies among the KPGs suggests the environments of these galaxies must have some level of similarity. For example, one may assume they are different structures forming in a common or comparable low-density environment: both form at the periphery of large-scale structures.

### 5.1.2. Intermediate-type (Sa–Sb) galaxies

In Figures 11 and 12, we show the variations in the Sa–Sb group of the isophotal parameters internal (Figure 11) and external (Figure 12) to  $r_0$ . In Figure 11, the KIGs tend to be slightly brighter than the KPGs and slightly bluer than the HCGs. This is confirmed by statistical tests (Table 10). However, the difference in luminosity may be due to the fact that there are no small-size Sa–Sb galaxies in the KIGs as compared to the KPGs and HCGs (clearly visible in Figure 11). Indeed, when we compare the magnitudes inside  $R_e$  the differences vanish (Table 11).

We see a trend for the HCGs to be redder than the KPGs or KIGs (Table 10). This suggests slightly older nuclear stellar populations in the HCG galaxies. However, statistical tests are inconclusive on this matter, except between the HCGs and KIGs inside  $r_0$ . The trend toward redder color for the HCG is also visible using  $R_e$ , but again statistical tests are inconclusive (Table 11).

Also from Figure 11 and Table 10 one can see that the KIG galaxies are more concentrated than the HCGs and KPGs inside  $r_0$ . In terms of  $R_{90\%}/R_{50\%}$ , the statistical tests only support a difference in concentration between the KIG and KPG galaxies (Table 11). However, the HCG galaxies are observed to have a greater  $R_e$  than the KIG galaxies (Table 11) and to have lower surface brightness at  $R_e$  (Table 11).

In Figure 12, the trend in concentration seems to continue outside  $r_0$ : the HCG galaxies seem less concentrated than the galaxies in the other two samples (Table 10). Also in Table 10 we find differences in surface brightness outside the half-radius, the HCGs and KPGs having higher surface brightness than the KIG galaxies.

The differences observed suggest different distributions in mass. In particular, the intermediate KIG galaxies seem smaller in size and more compact than the KPG and HCG galaxies. This may be explained by the isolation status of the KIG: stars in galaxies that have experienced interactions are expected to occupy higher energy orbits than those in galaxies that formed in isolation, and consequently isolated galaxies may be expected to be more compact or less spatially extended.

In Figure 11, no difference is observed in the asymmetry level. However, outside the half-

radius, Figure 12, the KPG galaxies tend to be slightly more asymmetric than the HCG galaxies, even though this is not confirmed by the statistical test (Table 10).

### 5.1.3. Late-type (*Sbc–Im*) galaxies

In Figures 13 and 14, we show the variations for the late-type galaxies of the isophotal parameters internal (Figure 13) and external (Figure 14) to  $r_0$ . In this group, we observe no obvious differences between the different parameters. The statistical tests (see Table 12) suggest small differences between the HCG and KIG galaxies in terms of magnitudes, with the KIG galaxies being slightly brighter than the HCG galaxies both inside  $r_0$  and  $R_e$ .

The HCG galaxies also seem to have lower surface brightness inside  $r_0$  than the KPG galaxies and to be less concentrated than the KIG galaxies outside  $r_0$ . The KPG galaxies seem to be bluer than the HCG inside  $R_e$  and to be smaller than the KIG galaxies. We do not find any other differences based on  $R_e$  among the samples (see Table 13). In terms of size and concentration, the trends seem to go contrary to what is observed for the intermediate types.

The most significant differences observed are in the level of asymmetry: the KIG galaxies turned out to be more symmetric than the KPG or the HCG galaxies. The asymmetry level does not seem significantly different between the HCG and KPG galaxies.

## 5.2. Origin of the asymmetries in galaxies

So far, our analysis has shown differences in the characteristics of the galaxies that are consistent with evidence for interaction effects due to their different environments. However, the fact that we observe different behaviors between morphology groups suggests we must be careful in our interpretation of asymmetries in terms of interactions. For example, in intermediate- and late-type spiral galaxy asymmetric features may be related to internal processes, like density waves or stochastic star formation propagation, which are not necessarily produced by interactions. Moreover, in multiple systems such as in compact groups (or clusters of galaxies), a sequence of interaction events may exist that are correlated with the morphol-

ogy of the galaxies: early-type galaxies, for example, may have entered the systems before late-type ones and would be expected to show less evidence of interactions than spirals for this reason.

In order to better determine the origin of the asymmetries observed in the various galaxies of our sample, we have meticulously reinspected the residual images produced by our asymmetry analysis and redistributed the galaxies in our sample in six different types of asymmetry, independent of the morphology. In type 1, we have put all the “symmetric” galaxies or galaxies with “intrinsic” asymmetries related to star formation clumps and/or spiral arms. Examples of galaxies with a type 1 asymmetry are shown in Figure 15. In type 2, we have regrouped all the galaxies where the asymmetry is possibly due to dust or to the inclination of the galaxy on the plane of the sky. Examples of galaxies with a type 2 asymmetry are presented in Figure 16. In type 3, we find the most obvious evidence of galaxy interactions under the forms of tidal tails, plumes, connecting bridges or a common envelop between galaxies. Examples of galaxies with a type 3 asymmetry are presented in Figure 17. We put galaxies that that are highly asymmetric, but for which the cause is not obvious in type 4. Examples of galaxies of this type can be found in Figure 18. In type 5, we have regrouped the cases where the asymmetry may be due to a smaller mass satellite galaxy. Examples of galaxies showing a type 5 asymmetry are shown in Figure 19. Finally, in type 6 we have regrouped the cases where the asymmetry is accompanied by a possible double nucleus. Examples of galaxies with this last type of asymmetry are shown in Figure 20.

The distribution of asymmetry types in the different samples is presented in Figure 21. In the KIG sample, 60% of the galaxies have an asymmetry of type 1 and 8% show an asymmetry of type 2. Therefore, slightly less than 70% of the KIG galaxies are unperturbed. In this group, we do find some “asymmetric” galaxies; however they are either of type 4 (19%) or of type 5 (13%). In general, and as expected, evidence of interactions is largely missing in the KIGs.

The contrast with the KPGs is significant; as much as 52% are classified as type 3, which are obvious cases of recent interactions. Of the remaining asymmetric galaxies, 8% are classified as

type 4, 6% as type 5 and another 3% as type 6. The rest of the galaxies are either type 1 (27%) or type 2 (4%). Therefore, almost 70% of the KPG galaxies show asymmetries consistent with “genuine” interactions.

In the case of the HCGs, 31% are classified as type 3, 6% as type 4, 6% as type 5, and 1% as type 6, summing up the evidence for genuine interactions to 44%. The number of “symmetric” galaxies, 44% of type 1 and 12% of type 2, is consequently higher than that in the KPGs.

## 6. Discussion and conclusion

Through our analysis we have found that galaxies in close pairs show more frequent signs of interactions at a higher level than those in compact groups. This may seem somewhat contradictory. If interaction between galaxies is favored in high-density environments with low velocity dispersion, should we not expect evidence for such processes to be more obvious in multiple systems like CGs? A possible answer to this apparent contradiction can be found in our isophotal analysis. Indeed, we have seen that the HCG galaxies tend to be redder in their central part and less compact in their periphery than the KPG galaxies, which is consistent with older central stellar populations and dynamically more relaxed orbits as a whole in the HCG galaxies than in the KPG galaxies. These observations, together with the presence of asymmetries at a lower level in the HCG galaxies, suggest CGs are found in a more advanced stage of interaction than pairs of galaxies. One possible explanation is that these structures formed at different epochs: CGs would have formed in the recent past, while close pairs would have formed even more recently.

The alternative interpretation is to assume that the evolution of galaxies is accelerated in CGs: the galaxies in CGs formed at the same time as those in close pairs, but they evolved faster due to multiple interactions. However, based on our observations, such an alternative seems less probable. In particular, we observe similar properties for the E–S0 in the HCGs and KPGs which suggest similar formation mechanisms. The higher number of such galaxies in the HCGs (see Figure 3), therefore, can only be the result of originally higher matter density: in denser regions, a high number of galaxies are formed, which can eventually inter-

act to build larger and more complex structures like CGs, while in less dense environments, a few galaxies are formed and it can take longer for these galaxies to interact with neighbors.

On the other hand, the fact that many S0 galaxies can also be found among the KPGs suggests their environment must have some level of similarity with that of the HCGs. The common property is that both systems are examples of structures forming in relatively low density environments; that is, both form relatively late at the periphery of large-scale structures.

The cosmological model that better fits our observations is one where the formation of structures is a biased process. As a consequence, it is expected that massive structures, which formed in originally denser regions, must assemble their components at earlier epochs than less massive ones. If we also assume the formation process of structures to be continuous in time, then we must now expect to observe smaller mass structures like CGs and pairs of galaxies to form at the periphery of the larger-scale structures.

## 7. ACKNOWLEDGMENTS

We thank the CATT of San Pedro Mártir for the observing time given on the 1.5 m telescope to realize this project and all the personnel of the observatory for their support. We also thank an anonymous referee for important comments and suggestions. This research has made use of SAOImage DS9, developed by the Smithsonian Astrophysical Observatory and FTOOLS (<http://heasarc.gsfc.nasa.gov/ftools/>), (Blackburn 1995), and TOPCAT software provided by the UK’s AstroGrid Virtual Observatory Project, which is funded by the Science and Technology Facilities Council and through the EU’s Framework 6 programs.

TABLE 1  
 PROPERTIES OF THE OBSERVED KIG GALAXIES

Name	R.A.	Decl.	$v_{vir}$	Morph.	$C$	$C$	$V - I$	$V - I$	$A$	$A$
(1)	(J2000) (2)	(J2000) (3)	(km s <sup>-1</sup> ) (4)	Type (5)	< $r_0$ (6)	> $r_0$ (7)	< $r_0$ (8)	> $r_0$ (9)	< $r_0$ (10)	> $r_0$ (11)
KIG 33	0 43 28	-00 07 30	4134	SBb*	0.96	2.41	1.15	1.08	1.01	1.06
KIG 53	1 30 47	21 26 26	3199	SBbc	0.49	1.37	1.09	1.03	1.01	1.10
KIG 56	1 36 00	00 39 49	5114	SBb	0.66	1.91	1.20	1.15	1.01	1.06
KIG 61	1 42 27	26 08 35	3986	SBab	1.76	0.90	1.31	1.41	1.00	1.18
KIG 68	1 53 13	04 11 45	1686	SBa	1.60	0.89	1.15	1.17	1.03	1.06
KIG 116	23 58 32	26 12 51	3363	SBab	1.16	2.13	1.12	1.05	1.04	1.11
KIG 123	3 12 51	04 42 25	5853	SBbc	0.68	0.74	1.25	1.38	1.00	1.05
KIG 467	11 09 16	36 01 16	6560	SB0	0.97	1.65	1.36	1.38	1.01	1.03
KIG 550	12 44 26	37 07 17	7193	SBbc	0.82	1.23	1.74	1.81	1.00	1.06
KIG 553	12 50 09	33 09 33	7273	SBb	1.29	1.60	0.86	0.91	1.00	1.03
KIG 575	13 12 07	24 05 42	2761	Sb	1.28	1.39	1.21	1.17	1.01	1.04
KIG 653	14 51 39	40 35 57	5138	Sb	0.89	1.45	1.40	1.37	1.01	1.03
KIG 716	15 57 28	30 03 36	10056	Sc	0.96	0.80	1.64	1.68	1.00	1.02
KIG 744	16 31 08	43 20 55	2854	Sc	0.87	1.21	0.95	0.90	1.02	1.10
KIG 748	16 33 48	28 59 05	1174	SBc*	0.63	0.15	1.09	1.17	1.04	1.12
KIG 805	17 23 47	26 29 11	4938	SBbc*	0.56	1.43	1.29	1.23	1.00	1.04
KIG 808	17 28 09	07 25 21	1812	SBc	0.23	0.66	1.29	1.34	1.00	1.02
KIG 812	17 32 40	16 24 05	3282	Sbc	0.83	0.72	1.37	1.31	1.01	1.16
KIG 838	17 52 06	21 34 09	6296	SBbc*	0.44	0.96	1.28	1.28	1.00	1.14
KIG 840	17 56 55	32 38 12	4978	SBbc	0.65	0.99	1.30	1.21	1.00	1.08
KIG 841	17 59 15	45 53 15	5658	S0	1.32	1.03	1.33	1.39	1.02	1.02
KIG 844	18 00 44	35 00 49	7450	Sbc	0.44	1.31	1.24	1.16	1.01	1.09
KIG 856	18 42 20	46 06 17	10148	SBbc	0.41	0.73	1.32	1.45	1.00	1.03
KIG 858	18 42 43	40 22 01	5735	SBbc	0.54	1.49	1.48	1.42	1.01	1.05
KIG 862	18 49 01	47 39 28	4930	Sbc	0.71	1.37	1.47	1.30	1.04	1.11
KIG 897	21 07 47	16 20 08	5090	Sa	1.22	0.31	1.28	1.24	1.05	1.07
KIG 924	21 41 30	00 53 41	4581	Sc	0.31	0.80	1.40	1.33	1.00	1.04
KIG 931	21 49 07	00 26 50	4780	SBbc	1.02	0.33	1.44	1.40	1.01	1.06
KIG 935	21 54 34	02 56 34	4024	SBc*	0.84	1.09	0.79	0.62	1.02	1.08
KIG 950	22 09 15	21 31 06	3928	Sc	0.74	0.78	1.31	1.04	1.01	1.13
KIG 967	22 28 26	30 17 29	1142	IBm*	0.58	0.43	0.62	1.12	1.13	1.14
KIG 983	22 43 52	38 22 37	4960	Sc	0.51	0.67	1.60	1.45	1.00	1.07
KIG 992	22 52 38	06 05 37	3540	Sc	0.52	0.69	1.47	1.50	1.01	1.09
KIG 1001	22 57 20	-01 02 57	3076	SBab	1.72	0.65	1.24	1.23	1.01	1.02
KIG 1009	23 12 26	34 52 53	5030	Sbc	0.51	1.75	1.18	1.10	1.00	1.06
KIG 1023	23 31 39	25 56 43	8147	SBb	0.95	1.78	1.42	1.44	1.00	1.03
KIG 1045	23 55 19	05 54 57	3883	S0	1.23	1.96	1.29	1.25	1.00	1.01

NOTE.—Columns: (1) catalog galaxy identification; (2) right ascension from HyperLeda (0<sup>h</sup>00<sup>m</sup>00<sup>s</sup>); (3) declination from HyperLeda (0°00′00″); (4) radial velocity corrected for infall Local Group toward Virgo from HyperLeda; (5) morphological type as determined in this work; (6) concentration inside  $r_0$ ; (7) concentration outside  $r_0$ ; (8) average  $V - I$  color inside  $r_0$ ; (9) average  $V - I$  color outside  $r_0$ ; (10) average asymmetry inside  $r_0$ ; and (11) average asymmetry outside  $r_0$ .

TABLE 2  
 PROPERTIES OF THE OBSERVED KPG GALAXIES

Name	R.A.	Decl.	$v_{vir}$	Morph.	$C$	$C$	$V - I$	$V - I$	$A$	$A$
(1)	(J2000) (2)	(J2000) (3)	( $\text{km s}^{-1}$ ) (4)	Type (5)	$< r_0$ (6)	$> r_0$ (7)	$< r_0$ (8)	$> r_0$ (9)	$< r_0$ (10)	$> r_0$ (11)
KPG 13A	0 36 52	23 59 27	4701	Sb	0.93	0.94	1.38	1.31	1.15	1.11
KPG 13B	0 36 52	23 59 05	4573	S0	0.93	0.52	0.70	0.75	1.08	1.17
KPG 61A	2 16 13	32 38 58	4916	Sb	0.68	2.20	1.33	1.16	1.02	1.09
KPG 61B	2 16 21	32 39 59	4752	SB0	1.27	1.02	1.22	1.18	1.01	1.01
KPG 75A	2 45 10	32 59 23	5099	SBa	1.34	1.23	1.30	1.30	1.01	1.11
KPG 75B	2 45 14	32 58 41	5169	SBb	0.57	0.72	1.29	1.26	1.05	1.20
KPG 99A	4 30 40	00 39 43	3590	E	1.47	0.59	1.28	1.26	1.03	1.18
KPG 99B	4 30 44	00 39 53	3411	E	1.50	0.63	1.24	1.20	1.04	1.13
KPG 313A	11 58 34	42 44 02	1014	SBc	1.56	0.69	1.63	1.64	1.02	1.06
KPG 313B	11 58 52	42 43 22	904	SBb	0.73	0.69	0.95	0.88	1.06	1.03
KPG 366A	13 13 26	27 45 49	6336	SB0	1.30	0.69	1.04	1.06	1.02	1.14
KPG 366B	13 13 27	27 48 09	6583	SBb	0.66	1.60	1.12	1.07	1.00	1.03
KPG 373A	13 24 51	36 22 43	5422	S0	1.35	1.49	0.77	0.78	1.00	1.04
KPG 373B	13 25 01	36 23 58	5824	S0	1.51	1.25	0.71	0.73	1.01	1.02
KPG 394A	13 46 19	43 51 05	2479	S0	0.88	0.99	1.09	1.14	1.00	1.03
KPG 394B	13 46 24	43 52 19	2642	SBc	0.56	0.94	1.41	1.30	1.02	1.11
KPG 397A	13 47 45	38 18 16	1631	Sc	1.90	1.18	1.08	1.07	1.09	1.18
KPG 397B	13 47 46	38 15 34	1644	Sb	0.55	1.02	1.06	1.04	1.01	1.09
KPG 404A	13 58 34	37 27 11	3685	SBb	1.72	0.51	...	...	1.10	1.11
KPG 404B	13 58 38	37 25 28	3684	SBb	0.67	0.76	...	...	1.05	1.58
KPG 432A	14 41 17	44 28 44	3536	S0	1.46	0.41	1.30	1.30	1.00	1.00
KPG 432B	14 41 32	44 30 46	3518	SBb	0.51	0.84	1.31	1.31	1.01	1.16
KPG 452A	15 05 55	12 44 40	6791	SB0	1.53	1.67	1.31	1.41	1.00	1.01
KPG 452B	15 05 56	12 43 41	6438	SB0	1.87	0.71	1.31	1.38	1.00	1.00
KPG 480B	16 04 31	03 52 06	5612	Sa	1.15	1.37	1.79	1.82	1.01	1.01
KPG 508A	17 19 14	48 58 49	7573	E	1.21	0.84	1.39	1.40	1.00	1.00
KPG 508B	17 19 21	49 02 26	7444	SBb pec	0.58	1.11	1.74	1.63	1.01	1.55
KPG 523A	17 46 08	35 34 10	6998	SBb	1.05	0.74	1.33	1.47	1.00	1.01
KPG 523B	17 46 17	35 34 19	6979	SBb	0.66	1.85	1.24	1.19	1.00	1.04
KPG 524A	17 46 28	30 42 17	4812	SBb	0.51	1.42	1.32	1.17	1.04	1.08
KPG 524B	17 46 32	30 41 54	4820	Sc	0.78	0.33	0.73	0.64	1.04	1.52
KPG 525A	17 49 11	20 48 16	3380	S0	1.36	0.33	1.39	1.46	1.00	1.01
KPG 525B	17 49 30	20 45 50	3523	SBc	0.64	1.14	1.31	1.23	1.01	1.10
KPG 526A	17 56 00	18 20 18	3171	Sa	1.29	1.06	1.40	1.42	1.00	1.02
KPG 526B	17 56 04	18 22 23	3047	S0	1.35	0.62	1.39	1.40	1.04	1.06
KPG 528A	17 59 58	26 21 19	5247	Sc	1.55	1.01	1.46	1.47	1.00	1.05
KPG 528B	18 00 05	26 22 00	4939	S0	0.72	0.67	1.29	1.36	1.00	1.00
KPG 537A	18 47 27	50 24 39	9325	SBa	0.62	1.20	1.30	1.25	1.00	1.02
KPG 537B	18 47 30	50 23 20	9219	E	1.19	1.13	1.26	1.22	1.01	1.05
KPG 539A	19 26 32	50 07 31	4331	S0	1.22	0.98	1.24	1.18	1.00	1.01
KPG 539B	19 26 37	50 08 18	4269	SBa	0.98	0.57	0.98	1.01	1.09	1.76
KPG 542A	19 31 08	54 06 08	4106	Sb	0.81	0.29	1.44	1.39	1.01	1.04
KPG 542B	19 31 10	54 05 33	3955	E	1.38	0.56	1.48	1.49	1.03	1.01
KPG 548A	20 47 19	00 19 15	4272	SBb	1.22	1.22	1.27	1.32	1.01	1.04
KPG 548B	20 47 24	00 18 03	3859	E	1.33	0.78	1.18	1.17	1.00	1.00
KPG 549A	20 51 22	18 58 41	8751	pec	0.68	1.58	1.26	1.21	1.01	1.16
KPG 549B	20 51 26	18 58 04	8833	SBb	0.44	1.53	1.68	1.39	1.06	1.04
KPG 551A	20 59 47	-01 53 15	5879	SBb	0.13	1.83	0.82	0.62	1.30	2.54
KPG 551B	20 59 48	-01 52 22	5868	SBc	1.00	0.55	0.93	0.92	1.02	1.18
KPG 552A	21 07 41	03 52 21	7836	SBa	0.44	1.35	1.37	1.30	1.00	1.08
KPG 552B	21 07 46	03 52 40	7925	S0	1.16	0.47	0.99	1.03	1.02	1.05
KPG 553A	21 08 21	18 12 00	5008	E	1.61	0.63	1.24	1.21	1.00	1.01
KPG 553B	21 08 27	18 11 27	5160	Sc	0.58	1.35	1.27	1.15	1.01	1.15
KPG 554A	21 09 36	15 07 30	9222	S0	1.05	1.80	1.25	1.19	1.00	1.01
KPG 554B	21 09 38	15 09 01	9027	S0	0.96	1.69	1.32	1.27	1.00	1.00
KPG 557A	21 28 58	11 21 59	8858	SBa	0.91	1.29	1.32	1.27	1.00	1.01

TABLE 2—*Continued*

Name	R.A.	Decl.	$v_{vir}$	Morph.	$C$	$C$	$V - I$	$V - I$	$A$	$A$
(1)	(J2000) (2)	(J2000) (3)	(km s <sup>-1</sup> ) (4)	Type (5)	< $r_0$ (6)	> $r_0$ (7)	< $r_0$ (8)	> $r_0$ (9)	< $r_0$ (10)	> $r_0$ (11)
KPG 557B	21 28 59	11 22 57	8634	Sc	0.39	1.39	1.11	1.00	1.00	1.44
KPG 566A	22 19 28	29 23 45	4782	Sc	0.37	0.50	1.78	1.54	1.11	1.07
KPG 566B	22 19 30	29 23 17	4654	Sd	0.47	0.25	1.70	1.43	1.10	1.15
KPG 572A	22 45 59	10 52 03	7626	SB0	1.75	1.19	1.17	1.16	1.02	1.01
KPG 572B	22 46 01	10 51 13	7152	Sb	0.61	1.05	1.13	1.06	1.00	1.11
KPG 573A	22 48 41	27 36 40	9733	Sb	0.68	2.32	1.23	1.17	1.01	1.11
KPG 573B	22 48 44	27 34 40	9729	SBc	0.30	1.88	1.26	0.97	1.02	1.15
KPG 575A	23 03 16	08 52 28	4950	Sa	1.29	1.80	1.11	1.24	1.02	1.04
KPG 575B	23 03 18	08 53 37	4934	pec	0.77	0.96	1.30	1.37	1.10	1.43
KPG 591A	23 46 59	29 27 32	5147	pec	1.43	0.54	0.87	0.88	1.87	1.15
KPG 591B	23 47 05	29 29 00	5294	SBb	0.81	1.09	1.27	1.14	1.00	1.08
KPG 598A	23 56 45	16 48 15	1898	Im	0.83	0.08	0.31	0.36	2.07	2.01
KPG 598B	23 56 45	16 48 43	1835	SBd pec	0.30	0.60	0.82	0.89	1.05	1.07
KPG 602A	0 01 27	31 26 02	5076	E	1.81	0.47	1.42	1.46	1.00	1.07
KPG 602B	0 01 30	31 26 32	4906	SBb	1.33	0.37	1.47	1.51	1.03	1.22

NOTE.—Columns: (1) catalog galaxy identification; (2) right ascension from HyperLeda (0<sup>h</sup>00<sup>m</sup>00<sup>s</sup>); (3) declination from HyperLeda (0°00′00″); (4) radial velocity corrected for infall Local Group toward Virgo from HyperLeda; (5) morphological type as determined in this work; (6) concentration inside  $r_0$ ; (7) concentration outside  $r_0$ ; (8) average  $V - I$  color inside  $r_0$ ; (9) average  $V - I$  color outside  $r_0$ ; (10) average asymmetry inside  $r_0$ ; and (11) average asymmetry outside  $r_0$ .

TABLE 3  
 PROPERTIES OF THE OBSERVED HCG GALAXIES

Name	R.A.	Decl.	$v_{vir}$	Morph.	$C$	$C$	$V - I$	$V - I$	$A$	$A$
(1)	(J2000) (2)	(J2000) (3)	( $\text{km s}^{-1}$ ) (4)	Type (5)	$< r_0$ (6)	$> r_0$ (7)	$< r_0$ (8)	$> r_0$ (9)	$< r_0$ (10)	$> r_0$ (11)
HCG 01a	0 26 07	25 43 31	10332	Sc	0.63	0.38	1.37	1.27	1.03	1.18
HCG 01b	0 26 06	25 43 10	10361	E	0.94	0.16	1.28	1.19	1.13	1.25
HCG 01c	0 25 54	25 43 24	10151	E	1.19	0.77	1.35	1.33	1.00	1.00
HCG 10a	1 26 22	34 42 11	5269	SBb	1.07	1.86	1.43	1.35	1.00	1.38
HCG 10c	1 26 19	34 45 15	4781	SB0	1.26	0.89	1.41	1.36	1.01	1.02
HCG 10d	1 26 31	34 40 32	4741	Scd	1.03	0.88	1.33	1.26	1.01	1.06
HCG 14a	1 59 52	-07 05 12	5261	SBb	0.58	1.23	1.40	1.34	1.00	1.04
HCG 14b	1 59 50	-07 03 33	5825	S0	0.97	0.77	1.23	1.16	1.00	1.03
HCG 14c	1 59 49	-07 01 53	5041	Sbc	0.59	0.83	1.33	1.28	1.03	1.03
HCG 15a	2 07 53	02 10 03	6907	S0	1.14	1.34	1.43	1.40	1.09	1.01
HCG 15b	2 07 34	02 06 55	7057	E	1.43	0.46	1.25	1.25	1.00	1.00
HCG 15c	2 07 40	02 08 58	7162	E-S0	1.38	0.78	1.23	1.23	1.00	1.00
HCG 15d	2 07 38	02 10 50	6184	E	1.28	0.44	1.25	1.25	1.00	1.01
HCG 15e	2 07 25	02 06 58	7137	E-S0	1.30	0.42	1.23	1.21	1.00	1.01
HCG 15f	2 07 38	02 11 25	6377	Sc	0.58	0.62	1.13	1.18	1.01	1.08
HCG 18b	2 39 05	18 23 20	4120	Im	0.50	0.19	0.80	0.82	1.02	1.06
HCG 24a	3 20 15	-10 51 47	9075	E-S0	0.99	0.87	1.31	1.31	1.00	1.00
HCG 24b	3 20 23	-10 52 02	8964	S0	0.95	0.72	1.31	1.29	1.00	...
HCG 24c	3 20 13	-10 51 48	9110	SB0	0.88	0.39	1.34	1.42	1.00	1.00
HCG 24d	3 20 20	-10 51 29	8605	SB0	1.84	0.30	1.23	...	1.00	...
HCG 25a	3 20 43	-01 06 31	6167	SBb	0.54	1.16	1.07	0.94	1.01	1.10
HCG 25b	3 20 45	-01 02 41	6290	S0	1.03	0.70	1.49	1.41	1.01	1.06
HCG 25d	3 20 39	-01 02 06	6284	S0	0.91	1.34	1.09	1.09	1.01	1.01
HCG 25f	3 20 45	-01 03 14	6161	S0	0.85	0.54	1.22	1.23	1.03	1.26
HCG 26a	3 21 56	-13 38 59	9489	Sc	0.36	0.44	1.55	1.32	1.05	1.46
HCG 26b	3 21 57	-13 38 56	9143	E	0.78	0.29	1.66	1.52	1.00	1.16
HCG 26c	3 21 49	-13 38 42	9429	S0	1.37	0.48	1.39	1.37	1.00	1.03
HCG 26d	3 21 56	-13 38 44	8944	E	0.75	0.29	1.07	1.03	1.00	1.06
HCG 26e	3 21 51	-13 39 51	9434	Sd	0.77	0.29	1.08	0.90	1.02	1.02
HCG 28a	4 27 19	-10 18 23	11228	Sb	0.71	1.23	...	...	1.01	1.28
HCG 28b	4 27 20	-10 19 34	11276	E	1.25	0.38	...	...	1.00	1.00
HCG 28c	4 27 18	-10 19 05	11077	S0	1.55	0.91	...	...	1.00	1.00
HCG 30a	4 36 19	-02 49 53	4531	SBa	0.99	1.18	1.39	1.34	1.00	1.05
HCG 30b	4 36 30	-02 51 59	4458	SBa	1.66	1.27	1.25	1.13	1.07	1.04
HCG 30c	4 36 23	-02 48 00	4342	SBb	0.66	0.38	0.72	0.70	1.07	1.02
HCG 31a	5 01 38	-04 15 28	3857	Sdm	1.19	0.19	0.76	0.75	2.20	1.50
HCG 31b	5 01 35	-04 15 50	3986	SBc	0.49	0.61	0.66	0.77	1.04	1.61
HCG 32a	5 01 45	-15 26 55	12279	E	1.07	1.03	1.27	1.29	1.00	1.03
HCG 32c	5 01 49	-15 25 50	11716	S0	0.73	0.88	1.30	1.21	1.00	1.00
HCG 32d	5 01 45	-15 25 50	12045	S0	1.11	0.94	1.31	1.38	1.00	1.00
HCG 34a	5 21 46	06 41 19	8902	E	1.22	1.18	0.78	0.78	1.00	1.00
HCG 34b	5 21 50	06 40 36	9525	SBa	0.89	0.75	1.27	0.98	1.05	1.31
HCG 34c	5 21 49	06 40 55	9297	SBb	0.47	0.84	0.45	0.44	1.00	...
HCG 34d	5 21 48	06 41 02	8722	S0	1.01	0.60	0.79	0.76	1.00	1.02
HCG 61a	12 12 19	29 10 46	3942	S0	1.54	1.26	1.35	1.33	1.00	1.00
HCG 61c	12 12 31	29 10 05	4114	SBbc	0.91	0.86	1.66	1.53	1.21	1.51
HCG 61d	12 12 27	29 08 57	4138	SB0	1.65	0.74	1.19	1.28	1.02	1.02
HCG 68a	13 53 27	40 16 59	2387	SB0	1.66	0.10	1.47	1.48	1.00	1.01
HCG 68b	13 53 27	40 18 14	2860	E	1.25	0.57	1.50	1.46	1.01	1.01
HCG 74a	15 19 25	20 53 46	12427	E	1.03	0.65	1.44	1.39	1.02	1.00
HCG 74b	15 19 24	20 53 27	12282	E	0.50	0.88	1.37	1.36	1.00	1.01
HCG 74c	15 19 26	20 53 58	12439	S0	0.96	0.72	1.42	1.36	...	...
HCG 79a	15 59 11	20 45 17	4469	E	0.73	0.60	1.53	1.43	1.00	1.00
HCG 79b	15 59 13	20 45 48	4623	SB0	0.72	0.97	1.31	1.28	1.00	1.02
HCG 79c	15 59 11	20 45 44	4323	SB0	0.88	0.43	1.16	1.19	1.01	1.03
HCG 82a	16 28 22	32 50 58	11398	S0	0.84	1.61	1.48	1.53	1.00	1.00

TABLE 3—Continued

Name	R.A.	Decl.	$v_{vir}$	Morph.	$C$	$C$	$V - I$	$V - I$	$A$	$A$
(1)	(J2000) (2)	(J2000) (3)	( $\text{km s}^{-1}$ ) (4)	Type (5)	$< r_0$ (6)	$> r_0$ (7)	$< r_0$ (8)	$> r_0$ (9)	$< r_0$ (10)	$> r_0$ (11)
HCG 82b	16 28 28	32 50 47	10668	SBa	0.71	1.58	1.59	1.57	1.00	1.00
HCG 82c	16 28 21	32 48 37	10316	Sd	0.31	1.20	1.66	1.45	1.02	1.17
HCG 82d	16 28 17	32 48 48	11906	Sa	1.23	0.73	1.40	1.39	1.00	1.01
HCG 86a	19 52 09	-30 49 32	6042	S0	1.30	0.91	1.47	1.51	1.00	1.00
HCG 86b	19 51 59	-30 48 58	6064	E	1.44	1.05	1.52	1.53	1.00	1.00
HCG 86c	19 51 57	-30 51 24	5396	SB0	1.36	0.71	1.52	1.47	1.00	1.02
HCG 86d	19 51 52	-30 48 31	5784	Sa	1.61	0.42	1.46	1.45	1.01	1.02
HCG 87a	20 48 15	-19 50 58	8587	SBc	0.52	0.90	1.57	1.44	1.04	1.15
HCG 87b	20 48 11	-19 51 23	8865	S0	1.22	0.35	1.29	1.22	1.00	1.02
HCG 87c	20 48 12	-19 49 56	8813	Sb	0.63	0.57	1.29	1.24	1.00	1.03
HCG 88a	20 52 36	-05 42 41	5970	Sb	0.69	0.99	1.37	1.25	1.03	1.04
HCG 88b	20 52 30	-05 44 46	5946	Sb	0.94	0.67	1.43	1.22	1.03	1.05
HCG 88c	20 52 26	-05 46 20	6019	Sc	0.67	0.36	1.13	1.06	1.02	1.09
HCG 88d	20 52 13	-05 47 54	5968	Sc	0.70	0.57	1.08	0.86	1.01	1.04
HCG 89a	21 20 01	-03 55 20	8801	SBb	0.47	0.40	1.19	1.07	1.00	1.09
HCG 89b	21 20 19	-03 53 46	8936	SBc	0.55	0.84	1.16	1.06	1.00	1.26
HCG 89c	21 20 08	-03 55 04	8823	SBc	0.84	0.53	1.04	0.91	1.00	1.02
HCG 89d	21 20 08	-03 54 29	8808	SBd	0.16	0.94	0.71	0.62	1.03	1.00
HCG 90a	22 02 02	-31 52 13	2429	Sb	0.91	0.76	1.53	1.29	1.27	1.03
HCG 90b	22 02 08	-31 59 25	2379	E	1.50	0.46	1.42	1.44	1.05	...
HCG 90c	22 02 03	-31 58 26	2550	E	1.58	0.48	1.42	1.46	1.00	1.01
HCG 90d	22 02 07	-31 59 32	2632	Sb pec	0.62	0.53	1.70	1.52	1.04	1.17
HCG 91a	22 09 08	-27 48 35	6700	SBb	0.90	0.98	1.26	1.31	1.02	1.14
HCG 91c	22 09 14	-27 46 56	7187	Sc	0.49	1.35	1.35	1.31	1.01	1.07
HCG 91d	22 09 09	-27 48 02	7063	SB0	1.18	1.01	1.39	1.35	1.00	1.00
HCG 92b	22 35 58	33 57 58	5925	SBb	0.62	0.47	1.25	1.23	1.01	1.01
HCG 92c	22 36 04	33 58 31	6915	SBb	0.72	1.06	1.37	1.30	1.00	1.25
HCG 92d	22 35 57	33 57 55	6781	S0	0.88	0.64	1.37	1.35	1.01	1.03
HCG 92e	22 35 52	33 56 42	6749	E	1.37	0.71	1.24	1.25	1.01	1.14
HCG 93a	23 15 16	18 57 41	5215	E	1.15	1.47	1.34	1.33	1.00	1.00
HCG 93b	23 15 17	19 02 29	4747	SBc	0.80	0.68	1.20	1.44	1.03	1.17
HCG 93c	23 15 03	18 58 25	5207	SBa	0.91	0.82	1.38	1.39	1.01	1.01
HCG 93d	23 15 33	19 02 53	5248	S0	1.13	1.01	1.32	1.27	1.00	1.02
HCG 94a	23 17 13	18 42 28	12113	E	1.13	0.72	1.31	1.34	1.00	1.00
HCG 94b	23 17 12	18 42 04	12047	E	1.03	0.50	1.30	1.36	1.00	1.00
HCG 94c	23 17 20	18 44 05	12193	Sa	0.84	1.11	1.30	1.33	1.01	1.02
HCG 94e	23 17 15	18 43 39	12323	Sd	0.40	1.03	1.64	1.45	1.01	1.03
HCG 94f	23 17 19	18 44 22	12993	S0	1.27	0.37	1.28	1.30	...	...
HCG 95a	23 19 30	09 30 29	11917	E	1.00	0.66	1.37	1.31	1.03	1.04
HCG 95b	23 19 35	09 29 42	11665	Sb	0.62	1.18	1.49	1.06	1.02	1.04
HCG 95c	23 19 31	09 30 11	11590	Sd pec	0.70	0.50	1.47	1.31	1.11	1.12
HCG 95d	23 19 28	09 29 40	12378	Sc	0.53	0.67	1.52	1.36	1.03	1.08
HCG 97a	23 47 23	-02 18 02	6879	E	0.81	1.38	1.40	1.44	1.00	1.00
HCG 97c	23 47 24	-02 21 06	5964	Sa	1.28	1.34	1.31	1.38	1.00	1.04
HCG 98a	23 54 10	00 22 58	7835	SB0	0.96	0.71	1.38	1.31	1.00	1.02
HCG 98b	23 54 12	00 22 38	7939	S0	1.24	0.35	1.44	1.32	1.02	1.09
HCG 98c	23 54 14	00 21 25	8125	E	1.22	1.33	1.53	1.29	1.00	1.00
HCG 99a	0 00 38	28 23 04	8818	Sa	0.87	0.69	1.37	1.34	1.01	1.04
HCG 99b	0 00 47	28 24 07	8959	E	1.21	0.90	1.35	1.29	1.01	1.02
HCG 99c	0 00 44	28 24 05	8329	SBb	0.75	0.38	1.36	1.37	1.02	1.06

NOTE.—Columns: (1) catalog Galaxy identification; (2) right ascension from HyperLeda ( $0^h00^m00^s$ ); (3) declination from HyperLeda ( $0^\circ00'00''$ ); (4) radial velocity from Hickson et al. (1992) and corrected for infall Local Group toward Virgo.; (5) morphological type as determined in this work; (6) concentration inside  $r_0$ ; (7) concentration outside  $r_0$ ; (8) average  $V - I$  color inside  $r_0$ ; (9) average  $V - I$  color outside  $r_0$ ; (10) average asymmetry inside  $r_0$ ; and (11) average asymmetry outside  $r_0$ .

TABLE 4  
 PROPERTIES OF OBSERVED VERSUS. CATALOG GALAXIES

Sample	$M_B$ (mag)	$P_{MW}$	$D_B$ (kpc)	$P_{MW}$	$V_{vir}$ (km s <sup>-1</sup> )	$P_{MW}$
(1)	(2)	(3)	(4)	(5)	(6)	(7)
KIG	-20.46/-20.30	0.070	25/22	0.153	4934/6296	<u>0.0003</u>
KPG	-20.35/-20.32	0.619	23/23	0.752	5123/6326	<u>0.0177</u>
HCG	-20.19/-20.01	0.119	26/24	0.050	7150/7970	0.6847

NOTE.—Columns: (1) sample identification; (2) median  $M_B$  value of the observed/catalog galaxies; (3) probability  $P$  for  $M_B$ ; (4) median value  $D_B$  of the observed/catalog galaxies; (5) probability  $P$  for  $D_B$ ; (6) median  $v_{vir}$  value of the observed/catalog galaxies; and (7) probability  $P$  for  $v_{vir}$ .  $P$  values were obtained from Mann–Whitney tests. Underlined values indicate statistically significant differences between two samples.

TABLE 5  
 OBSERVING RUNS

Run	Date	CCD	Filters	Seeing (FWHM)	$\sigma_V$ (mag)	$\sigma_I$ (mag)
(1)	(2)	(3)	(4)	(5)	(6)	(7)
1	2005 Oct	Site1	$V, I$	2.4''	$\pm 0.02$	$\pm 0.03$
2	2006 Aug	Site1	$V, I$	1.6''	$\pm 0.03$	$\pm 0.05$
3	2007 Sep	Marconi	$V, I$	1.9''	$\pm 0.03$	$\pm 0.04$
4	2008 May	Site1	$V, I$	1.8''	$\pm 0.11$	$\pm 0.08$
5	2008 Jul	Site1	$V, I$	1.4''	$\pm 0.05$	$\pm 0.04$

NOTE.—Columns: (1) running number; (2) observation dates; (3) CCD detectors; (4) filters; (5) average seeing; (6) and (7) calibration uncertainties for  $V$  and  $I$ , respectively

TABLE 6  
 PROPERTIES OF OBSERVED GALAXIES USING EFFECTIVE RADIUS ( $1/\eta(R_P) = 0.2$ )

Name	Morph. (type)	$R_P$ (arcsec)	$R_P$ (kpc)	$R_e$ (arcsec)	$R_e$ (kpc)	$M_e V$ (mag)	$M_e I$ (mag)	$R_{90}/R_{50}$	$\mu_V$ (mag arcsec $^{-2}$ )	$V - I$ (mag)
(1)	(2)	(3)	(4)	(5)	(6)	(7)	(8)	(9)	(10)	(11)
KIGs										
KIG 33	SBb*	21.0	6	11.6	3	-19.57	-20.59	1.7	20.5	1.02
KIG 53	SBbc	40.3	8	25.4	5	-19.42	-20.32	1.4	21.9	0.91
KIG 56	SBb	20.7	7	9.2	3	-19.61	-20.60	2.2	20.9	0.99
KIG 61	SBab	10.8	3	3.3	1	-19.19	-20.39	2.8	19.0	1.19
KIG 68	SBa	11.2	1	4.1	<1	-18.20	-19.27	2.3	18.6	1.08
KIG 116	SBab	23.2	5	11.5	2	-19.41	-20.40	1.9	20.3	0.99
KIG 123	SBbc	70.0	26	35.9	14	-21.17	-22.13	1.7	21.7	0.97
KIG 467	SB0	18.8	8	6.0	3	-20.07	-21.38	2.4	20.3	1.32
KIG 550	SBbc	38.8	18	24.9	12	-20.86	-22.66	1.4	22.2	1.81
KIG 553	SBb	21.8	1	7.9	4	-20.73	-21.07	3.8	20.9	0.33
KIG 575	Sb	32.6	6	15.2	3	-19.39	-20.50	1.8	20.7	1.12
KIG 653	Sb	29.6	1	12.3	4	-20.39	-21.66	2.1	20.9	1.28
KIG 744	Sc	18.8	3	9.3	2	-17.24	-18.12	1.9	21.8	0.88
KIG 805	SBbc*	32.6	1	15.3	5	-19.81	-20.97	1.8	21.3	1.16
KIG 812	Sbc	58.9	12	25.0	5	-20.18	-21.33	2.1	21.4	1.15
KIG 838	SBbc*	34.2	14	20.3	8	-20.63	-21.88	1.5	21.6	1.26
KIG 840	SBbc	38.8	12	16.0	5	-20.09	-21.20	2.1	21.6	1.12
KIG 841	S0	17.2	6	6.5	2	-20.29	-21.64	2.3	19.7	1.36
KIG 844	Sbc	25.0	12	12.0	6	-19.61	-20.61	1.8	22.0	1.00
KIG 856	SBbc	24.7	16	17.4	11	-20.38	-21.65	1.2	22.4	1.26
KIG 858	SBbc	27.8	1	15.0	6	-20.08	-21.34	1.6	20.8	1.25
KIG 862	Sbc	28.0	9	13.0	4	-19.94	-21.12	1.8	21.1	1.19
KIG 897	Sa	12.0	4	4.9	2	-20.46	-21.60	2.1	19.0	1.14
KIG 935	SBc*	31.6	8	16.9	4	-20.19	-20.63	1.6	21.2	0.44
KIG 950	Sc	43.2	11	21.1	5	-19.21	-20.18	1.8	22.2	0.97
KIG 1001	SBab	17.1	3	6.2	1	-19.08	-20.17	2.5	20.2	1.09
KIG 1009	Sbc	24.6	8	11.9	4	-20.17	-21.18	1.8	20.9	1.01
KIG 1023	SBb	25.0	13	8.4	4	-20.70	-21.98	3.0	20.9	1.27
KIG 1045	S0	17.9	4	7.4	2	-20.40	-21.59	2.1	19.1	1.20
KPGs										
KPG 013A	Sb	28.9	9	13.2	4	-19.23	-20.34	1.9	21.2	1.11
KPG 061A	Sb	34.2	11	17.8	6	-20.07	-21.12	1.7	21.3	1.05
KPG 061B	SB0	7.0	2	2.5	1	-18.42	-19.50	2.3	19.4	1.09
KPG 075A	SBa	11.2	4	4.0	1	-19.60	-20.80	2.4	19.3	1.21
KPG 075B	SBb	25.8	9	11.9	4	-19.19	-20.39	2.0	21.1	1.21
KPG 099A	E	13.4	3	5.7	1	-20.11	-21.34	2.1	18.9	1.24
KPG 099B	E	6.16	1	2.8	1	-18.76	-19.92	1.9	18.4	1.17
KPG 313A	SBc	57.3	4	31.1	2	-17.27	-18.08	1.7	22.1	0.81
KPG 313B	SBb	31.1	2	15.0	1	-17.32	-18.92	1.8	19.5	1.60
KPG 366A	SB0	15.7	6	5.1	2	-19.13	-20.20	2.4	20.9	1.07
KPG 366B	SBb	29.6	13	17.0	7	-20.64	-21.60	1.5	21.3	0.96
KPG 373A	S0	11.1	4	4.5	2	-20.07	-20.75	2.1	19.2	0.68
KPG 373B	S0	9.5	4	4.5	2	-19.91	-20.52	1.7	19.1	0.61
KPG 394A	S0	21.8	3	8.2	1	-17.29	-18.37	2.3	21.6	1.08
KPG 394B	SBc	83.5	14	34.3	6	-20.00	-21.10	2.1	21.2	1.10
KPG 397A	Sc	21.8	2	10.5	1	-17.79	-18.77	1.8	19.8	0.98
KPG 397B	Sb	18.8	2	9.1	1	-16.09	-17.13	1.7	21.1	1.04
KPG 404A	SBb	12.6	3	6.8	2	-18.49	...	1.7	20.5	...
KPG 404B	SBb	63.5	15	39.5	9	-20.30	...	1.5	20.6	...
KPG 432A	S0	9.5	2	3.6	1	-18.48	-19.73	2.2	19.5	1.26
KPG 452A	SB0	9.5	4	3.0	1	-19.32	-20.57	2.6	19.3	1.25
KPG 452B	SB0	9.5	4	3.1	1	-19.17	-20.50	2.5	19.5	1.34
KPG 480B	Sa	18.8	7	5.1	2	-20.13	-21.87	2.9	19.5	1.74
KPG 508A	E	9.8	5	3.1	2	-19.64	-20.95	2.6	20.1	1.31
KPG 508B	Sbbpec	36.1	17	13.8	7	-20.39	-21.72	2.2	21.3	1.33

TABLE 6—Continued

Name	Morph. (type)	$R_P$ (arcsec)	$R_P$ (kpc)	$R_e$ (arcsec)	$R_e$ (kpc)	$M_e V$ (mag)	$M_e I$ (mag)	$R_{90}/R_{50}$	$\mu_V$ (mag arcsec $^{-2}$ )	$V - I$ (mag)
(1)	(2)	(3)	(4)	(5)	(6)	(7)	(8)	(9)	(10)	(11)
KPG 523B	SBb	18.2	8	9.1	4	-20.15	-21.23	1.7	20.7	1.08
KPG 524A	SBb	19.8	6	14.0	4	-19.24	-20.28	1.4	20.8	1.03
KPG 524B	Sc	18.2	6	7.0	2	-17.24	-17.93	2.3	21.8	0.68
KPG 525A	S0	16.7	4	5.4	1	-18.90	-20.35	2.6	20.0	1.44
KPG 525B	SBc	38.3	9	18.3	4	-19.49	-20.58	1.8	21.4	1.08
KPG 526A	Sa	11.1	2	4.3	1	-19.43	-20.85	2.1	19.0	1.42
KPG 526B	S0	23.4	5	7.6	1	-19.64	-20.91	2.5	19.7	1.27
KPG 528A	Sc	16.7	6	7.8	3	-18.63	-19.86	1.9	21.7	1.23
KPG 528B	S0	13.6	4	4.2	1	-19.92	-21.33	2.9	19.5	1.41
KPG 537A	SBa	17.6	11	7.6	5	-19.68	-20.88	2.0	21.2	1.20
KPG 537B	E	6.7	4	2.9	2	-19.81	-21.03	2.0	19.9	1.22
KPG 539A	S0	13.4	4	4.3	1	-19.59	-20.73	2.7	19.1	1.14
KPG 539B	SBa	13.2	4	6.0	2	-18.19	-19.27	1.9	20.9	1.08
KPG 542B	E	9.5	2	3.3	1	-18.95	-20.38	2.4	18.9	1.43
KPG 548A	SBb	11.8	3	4.9	1	-19.89	-21.20	2.1	19.2	1.31
KPG 548B	E	12.6	3	5.4	1	-19.45	-20.60	2.0	19.5	1.15
KPG 549A	pec	13.6	8	7.0	4	-19.56	-20.60	1.7	21.0	1.04
KPG 549B	SBb	22.9	13	11.5	7	-20.82	-22.13	1.6	20.5	1.31
KPG 551A	SBb	16.5	6	8.1	3	-19.07	-19.76	1.9	21.7	0.70
KPG 551B	SBc	10.6	4	4.3	2	-18.25	-19.35	2.2	21.1	1.10
KPG 552A	SBa	26.0	13	11.8	6	-20.45	-21.58	1.8	21.2	1.13
KPG 552B	S0	10.5	5	4.1	2	-19.92	-20.94	3.9	21.0	1.02
KPG 553A	E	6.7	2	3.0	1	-19.24	-20.38	2.0	19.3	1.14
KPG 553B	Sc	30.2	1	13.0	4	-18.96	-20.07	2.0	21.5	1.11
KPG 554A	S0	8.4	5	3.5	2	-20.18	-21.32	2.1	19.7	1.15
KPG 554B	S0	10.1	6	4.4	3	-20.47	-21.73	2.0	19.9	1.26
KPG 557A	SBa	12.3	7	4.2	2	-19.40	-20.63	2.6	20.6	1.24
KPG 557B	Sc	21.0	12	12.9	7	-20.36	-21.23	1.4	21.5	0.87
KPG 566A	Sc	32.6	1	18.0	6	-19.38	-20.57	1.7	21.4	1.19
KPG 572A	SB0	5.6	3	2.3	1	-19.39	-20.54	2.1	19.0	1.15
KPG 572B	Sb	19.9	9	9.3	4	-20.10	-21.08	1.9	21.3	0.98
KPG 573A	Sb	14.0	9	6.3	4	-20.04	-21.03	1.9	20.9	0.99
KPG 573B	SBc	29.0	18	13.8	9	-21.38	-22.06	1.8	21.6	0.68
KPG 575A	Sa	10.8	3	2.7	1	-20.46	-21.72	3.4	18.2	1.25
KPG 575B	pec	22.9	7	11.5	4	-19.40	-20.64	1.7	21.0	1.23
KPG 591A	pec	14.0	5	6.8	2	-19.34	-20.20	1.8	20.1	0.86
KPG 591B	SBb	48.7	17	25.8	9	-21.34	-22.07	1.8	21.4	0.73
KPG 598A	Im	9.3	1	4.7	1	-15.52	...	1.8	21.7	...
KPG 598B	Sbdpec	20.1	2	11.6	1	-16.88	-17.66	1.6	21.6	0.78
KPG 602A	E	8.3	3	3.1	1	-19.53	-20.88	2.2	19.0	1.35
KPG 602B	SBb	11.4	4	4.5	1	-19.23	-20.57	2.2	19.9	1.34
HCGs										
HCG 01c	E	9.1	6	3.0	2	-19.64	-20.97	2.6	20.5	1.33
HCG 10a	SBb	38.9	13	13.7	5	-20.70	-22.04	2.4	20.9	1.34
HCG 10c	SB0	19.4	6	6.5	2	-19.14	-20.50	2.2	20.8	1.36
HCG 10d	Scd	24.0	7	10.5	3	-18.42	-19.67	1.9	21.3	1.25
HCG 14a	SBb	23.0	9	9.5	4	-19.32	-20.65	2.1	21.7	1.33
HCG 14b	S0	24.5	8	9.8	3	-19.50	-20.73	2.2	21.5	1.23
HCG 15a	S0	13.7	6	4.6	2	-19.75	-21.20	2.4	20.2	1.45
HCG 15b	E	8.6	4	3.2	1	-19.56	-20.89	2.2	19.8	1.33
HCG 15c	E-S0	9.6	4	3.6	2	-19.77	-21.06	2.2	20.1	1.29
HCG 15d	E	13.2	5	5.0	2	-19.18	-20.44	2.2	20.8	1.26
HCG 15e	E-S0	10.6	5	4.0	2	-19.15	-20.40	2.2	20.8	1.25
HCG 24a	E-S	13.7	8	6.7	4	-20.05	-21.49	1.7	21.5	1.44
HCG 24b	S0	15.8	9	5.0	3	-19.96	-21.37	2.5	20.7	1.41
HCG 24d	SB0	6.5	4	2.7	2	-17.91	-19.13	2.0	21.1	1.22
HCG 25a	SBb	37.4	15	16.3	6	-19.78	-20.49	1.8	21.8	0.72

TABLE 6—*Continued*

Name	Morph.	$R_P$	$R_P$	$R_e$	$R_e$	$M_e V$	$M_e I$	$R_{90}/R_{50}$	$\mu_V$	$V - I$
(1)	(type)	(arcsec)	(kpc)	(arcsec)	(kpc)	(mag)	(mag)	(9)	(mag arcsec <sup>-2</sup> )	(mag)
HCG 25b	S0	19.4	8	7.3	3	-19.78	-21.18	2.2	20.8	1.40
HCG 25d	S0	9.1	4	4.0	2	-18.52	-19.65	1.9	20.7	1.14
HCG 26c	S0	8.1	5	2.9	2	-18.42	-19.82	2.2	20.8	1.40
HCG 28a	Sb	22.5	16	6.9	5	-19.95	-19.68	2.6	21.4	-0.26
HCG 28b	E	9.1	7	2.9	2	-19.65	-19.51	2.4	20.5	-0.13
HCG 28c	S0	6.0	4	2.2	2	-19.41	-19.29	2.1	19.8	-0.12
HCG 30a	SBa	24.6	7	9.6	3	-19.98	-21.20	2.4	20.7	1.23
HCG 30b	SBa	13.4	4	5.6	2	-19.50	-20.64	2.1	19.6	1.15
HCG 32a	E	12.2	1	4.6	4	-20.95	-22.30	2.3	20.5	1.35
HCG 32c	S0	12.7	1	5.7	4	-19.51	-20.71	1.9	22.4	1.20
HCG 32d	S0	9.1	7	3.2	3	-19.76	-21.26	2.3	20.6	1.50
HCG 34a	E	10.1	6	4.0	2	-20.95	-21.76	2.2	19.4	0.81
HCG 34b	SBa	11.7	7	5.8	4	-18.95	-19.94	1.7	21.1	0.99
HCG 34d	S0	6.5	4	2.2	1	-17.97	-18.71	2.3	20.9	0.74
HCG 61a	S0	15.7	4	6.2	2	-20.07	-21.35	2.0	18.7	1.28
HCG 61c	SBbc	41.9	11	15.4	4	-19.58	-21.00	2.2	20.9	1.42
HCG 61d	SB0	14.1	4	3.8	1	-19.24	-20.40	3.3	18.8	1.17
HCG 68a	SB0	24.9	4	11.0	2	-20.12	-21.54	2.0	18.7	1.42
HCG 68b	E	18.8	3	8.7	2	-19.83	-21.32	1.8	19.4	1.49
HCG 79b	SB0	11.1	3	5.0	1	-19.13	-20.35	1.9	19.2	1.23
HCG 82a	S0	15.0	11	5.8	4	-20.95	-22.44	2.2	20.5	1.49
HCG 82b	SBa	14.5	1	6.8	5	-20.47	-21.91	1.9	21.0	1.44
HCG 82c	Sd	17.7	12	8.5	6	-19.66	-20.80	1.8	21.3	1.14
HCG 82d	Sa	8.3	6	2.4	2	-19.38	-20.65	2.6	20.2	1.27
HCG 86a	S0	14.5	6	5.8	2	-20.58	-22.00	2.2	19.2	1.42
HCG 86b	E	11.5	5	4.6	2	-20.10	-21.52	2.1	19.5	1.42
HCG 86c	SB0	12.6	4	4.9	2	-19.28	-20.66	2.2	20.3	1.38
HCG 86d	Sa	9.8	4	2.9	1	-19.20	-20.53	2.8	19.0	1.32
HCG 87a	SBc	35.8	2	13.3	7	-20.36	-21.70	2.2	21.4	1.34
HCG 87b	S0	11.2	6	3.8	2	-20.09	-21.21	2.4	20.3	1.12
HCG 87c	Sb	11.7	7	6.5	4	-18.58	-19.81	1.7	21.6	1.23
HCG 88a	Sb	36.3	14	15.8	6	-20.55	-21.49	1.9	21.0	0.95
HCG 88b	Sb	25.5	1	12.0	5	-20.34	-21.56	1.7	21.2	1.23
HCG 89d	SBd	9.6	5	6.3	4	-18.15	-18.61	1.3	21.9	0.46
HCG 90a	Sb	48.9	8	24.2	4	-19.69	-20.74	1.8	21.0	1.05
HCG 90b	E	12.4	2	4.5	1	-19.32	-20.66	2.3	18.5	1.34
HCG 90c	E	10.9	2	4.2	1	-19.18	-20.53	2.2	18.4	1.35
HCG 91a	SBb	21.6	9	10.3	4	-20.88	-22.01	1.8	20.4	1.13
HCG 91c	Sc	20.0	9	10.8	5	-19.70	-21.01	1.6	21.7	1.30
HCG 91d	SB0	7.7	4	2.2	1	-19.48	-20.74	2.9	18.9	1.25
HCG 92c	SBb	26.0	12	11.3	5	-20.26	-21.46	2.2	21.1	1.20
HCG 92d	S0	6.7	3	2.7	1	-19.85	-21.11	2.1	18.8	1.27
HCG 92e	E	6.7	3	3.1	1	-19.63	-20.85	1.9	19.2	1.23
HCG 93a	E	17.0	6	6.8	2	-20.85	-22.09	2.3	19.5	1.24
HCG 93b	SBc	42.0	13	17.4	5	-20.10	-21.25	2.0	21.4	1.15
HCG 93c	SBa	26.2	9	9.3	3	-20.11	-21.36	2.3	20.4	1.24
HCG 93d	S0	9.6	3	3.3	1	-18.98	-20.24	2.6	19.9	1.27
HCG 94c	Sa	15.3	12	4.9	4	-20.21	-21.58	2.5	21.0	1.38
HCG 94f	S0	7.6	6	2.6	2	-18.59	-19.91	2.3	21.6	1.32
HCG 95a	E	12.7	1	4.5	3	-20.86	-22.17	2.4	20.3	1.32
HCG 95b	Sb	15.8	12	7.1	5	-19.93	-20.93	1.9	21.4	1.00
HCG 97a	E	21.6	1	8.5	4	-20.61	-22.05	2.2	20.7	1.44
HCG 97c	Sa	12.3	5	5.0	2	-19.59	-20.87	2.2	20.1	1.28
HCG 98a	SB0	17.8	9	6.8	3	-20.77	-22.09	2.2	19.8	1.33
HCG 98b	S0	11.7	6	3.7	2	-19.95	-21.30	2.5	19.8	1.35
HCG 98c	E	6.0	3	2.5	1	-18.76	-20.06	2.0	20.1	1.30
HCG 99b	E	10.6	6	4.0	2	-20.51	-22.04	2.3	20.0	1.54

TABLE 6—*Continued*

Name	Morph. (type)	$R_P$ (arcsec)	$R_P$ (kpc)	$R_e$ (arcsec)	$R_e$ (kpc)	$M_e V$ (mag)	$M_e I$ (mag)	$R_{90}/R_{50}$	$\mu_V$ (mag arcsec <sup>-2</sup> )	$V - I$ (mag)
(1)	(2)	(3)	(4)	(5)	(6)	(7)	(8)	(9)	(10)	(11)
HCG 99c	SBb	18.9	1	9.1	5	-19.73	-21.22	1.9	21.9	1.49

NOTE.—Columns: (1) catalog galaxy identification; (2) morphological type as determined in this work; (3) petrosian radius defined as  $1/\eta(R_P) = 0.2$ ; (4) petrosian radius in kiloparsec; (5) effective radius  $R_e$ ; (6) effective radius in kiloparsec; (7) absolute magnitude in  $V$  inside  $R_e$ ; (8) absolute magnitude in  $I$  inside  $R_e$ ; (9) concentration index, defined as the ratio of radii that contain 90% and 50% of the Petrosian flux; (10) surface brightness at  $R_e$ ; and (11) color at  $R_e$ .

TABLE 7  
 PROPERTIES OBSERVED GALAXIES USING EFFECTIVE RADIUS ( $1/\eta(R_P) = 0.4$ )

Name	Morph. (type)	$R_P$ (arcsec)	$R_P$ (kpc)	$R_e$ (arcsec)	$R_e$ (kpc)	$M_e V$ (mag)	$M_e I$ (mag)	$R_{90}/R_{50}$	$\mu_V$ (mag arcsec $^{-2}$ )	$V - I$ (mag)
(1)	(2)	(3)	(4)	(5)	(6)	(7)	(8)	(9)	(10)	(11)
KIGs										
KIG 716	Sc	4.9	3	2.0	1	-19.08	-20.68	2.3	19.9	1.60
KIG 748	SBc*	45.0	3	26.0	2	-16.64	-17.54	1.6	22.2	0.90
KIG 808	SBc	26.2	3	15.5	2	-16.96	-18.65	1.6	21.1	1.69
KIG 924	Sc	29.3	9	18.7	6	-19.23	-20.30	1.5	22.1	1.06
KIG 931	SBbc	15.4	5	12.9	4	-18.56	-19.51	1.2	21.8	0.95
KIG 967	Sc	41.4	3	24.4	2	-16.86	-17.54	1.6	21.3	0.68
KIG 983	Sc	35.5	11	21.6	7	-19.93	-21.31	1.5	21.6	1.38
KIG 992	Sc	32.4	7	18.7	4	-18.59	-19.84	1.7	22.3	1.24
KPGs										
KPG 013B	S0	7.3	2	3.4	1	-17.76	-18.47	1.9	19.9	0.71
KPG 432B	SBb	29.6	7	20.3	5	-19.34	-20.55	1.4	21.3	1.21
KPG 523A	SBb	7.5	3	2.9	1	-18.95	-20.19	2.5	19.9	1.23
KPG 542A	Sb	24.9	7	12.2	3	-19.50	-20.89	1.8	21.0	1.39
HCGs										
HCG 01a	Sc	15.2	1	7.1	5	-19.75	-20.54	1.9	21.4	0.80
HCG 01b	E	4.5	3	2.4	2	-19.11	-20.40	1.6	20.2	1.29
HCG 14c	Sbc	10.6	3	5.1	2	-17.61	-18.85	1.9	20.9	1.24
HCG 15f	Sc	13.2	5	5.9	2	-17.72	...	2.0	22.2	...
HCG 24c	SB0	7.6	4	3.2	2	-18.37	-20.09	2.1	21.2	1.72
HCG 25f	S0	5.5	2	3.0	1	-17.79	-19.14	1.6	20.8	1.35
HCG 26a	Sc	20.4	13	11.5	7	-19.34	-20.38	1.6	22.1	1.04
HCG 26b	E	7.0	4	3.2	2	-18.73	-19.87	2.0	21.0	1.14
HCG 26d	E	4.5	3	2.2	1	-17.68	-18.80	1.8	21.1	1.12
HCG 26e	Sd	9.1	6	4.6	3	-17.41	-18.23	1.8	22.2	0.82
HCG 30c	SBb	12.7	4	6.0	2	-17.27	-17.96	1.7	21.6	0.69
HCG 31a	Sdm	16.3	4	8.1	2	-17.83	-18.57	1.8	20.3	0.75
HCG 31b	SBc	16.3	4	8.6	2	-17.36	-18.05	1.7	21.3	0.69
HCG 34c	SBb	7.6	5	3.8	2	-18.46	-18.88	1.8	21.1	0.43
HCG 74a	E	6.4	5	3.0	2	-20.62	-21.97	1.7	19.2	1.35
HCG 74b	E	4.9	4	3.0	2	-20.05	-21.36	1.4	19.6	1.31
HCG 74c	S0	4.9	4	2.5	2	-19.31	-20.62	1.7	20.1	1.32
HCG 79a	E	9.5	3	4.3	1	-18.60	-19.84	2.1	19.9	1.24
HCG 79c	SB0	8.0	2	4.3	1	-17.91	-19.02	1.7	19.9	1.11
HCG 88c	Sc	15.3	6	7.9	3	-19.10	-20.10	1.8	21.7	1.00
HCG 88d	Sc	14.8	6	8.6	3	-18.42	-19.35	1.5	21.5	0.93
HCG 89a	SBb	24.0	14	13.7	8	-19.81	-20.71	1.6	22.1	0.90
HCG 89b	SBc	16.3	9	6.9	4	-19.12	-20.16	2.1	22.1	1.04
HCG 89c	SBc	11.2	6	6.0	3	-18.68	-19.40	1.6	21.8	0.72
HCG 90d	Sb pec	21.2	4	11.5	2	-18.94	-20.22	1.6	19.6	1.27
HCG 92b	SBb	3.6	1	1.8	1	-18.80	-19.89	1.8	18.6	1.09
HCG 94a	E	5.5	4	2.9	2	-20.44	-21.89	1.7	19.5	1.45
HCG 94b	E	5.5	4	2.5	2	-19.97	-21.42	1.8	19.9	1.45
HCG 94c	Sd	9.6	8	6.0	5	-18.18	-19.67	1.4	22.0	1.49
HCG 95c	Sd pec	9.6	7	5.0	4	-19.45	-20.49	1.7	21.4	1.05
HCG 95d	Sc	13.7	11	5.6	4	-19.08	-20.32	2.1	21.5	1.24
HCG 99a	Sa	8.1	5	3.2	2	-19.79	-21.40	2.1	19.7	1.61

NOTE.—Columns: (1) catalog galaxy identification; (2) morphological type as determined in this work; (3) petrosian radius defined as  $1/\eta(R_P) = 0.4$ ; (4) petrosian radius in kiloparsec; (5) effective radius,  $R_e$ ; (6) effective radius in kiloparsec; (7) absolute magnitude in  $V$  inside  $R_e$ ; (8) absolute magnitude in  $I$  inside  $R_e$ ; (9) concentration index, defined as the ratio of radii that contain 90% and 50% of the Petrosian flux; (10) surface brightness at  $R_e$ ; and (11) color at  $R_e$ .

TABLE 8  
 PROPERTIES OF EARLY-TYPE GALAXIES IN DIFFERENT ENVIRONMENTS

Property (1)	HCGs (2)	KPGs (3)	$P_{MW}$ (4)
$M_V$	-20.3	-20.4	0.4006
$M_I$	-21.7	-21.5	0.0992
$\mu_{<r_0}$	20.4	20.4	0.2233
$\mu_{>r_0}$	22.4	23.0	<u>0.0026</u>
$(V - I)_{<r_0}$	1.34	1.25	<u>0.0017</u>
$(V - I)_{>r_0}$	1.33	1.21	<u>0.0100</u>
$C_{<r_0}$	1.1	1.4	<u>0.0040</u>
$C_{>r_0}$	0.7	0.7	0.1193
$A_{<r_0}$	1.00	1.00	0.0716
$A_{>r_0}$	1.01	1.01	0.0830

NOTE.—Columns: (1) properties measured in each sample (all values are medians): absolute magnitude in  $V$  inside  $r_0$ , absolute magnitude in  $I$  inside  $r_0$ , surface brightness in  $V$  inside and outside  $r_0$ ,  $V - I$  color inside and outside  $r_0$ , concentration index inside and outside  $r_0$ , asymmetry level inside and outside  $r_0$ ; (2) and (3) galaxies in HCGs and KPGs, respectively; (4)  $P$  values from Mann–Whitney tests, where underlined values indicate statistically significant differences.

TABLE 9  
 PROPERTIES OF EARLY-TYPE GALAXIES AS MEASURED USING  $R_e$

Property (1)	HCGs (2)	KPGs (3)	$P_{MW}$ (4)
$M_V$	-20.4	-20.2	0.0669
$M_I$	-21.7	-21.3	<u>0.0368</u>
$\mu_V$	20.2	19.5	<u>0.0124</u>
$(V - I)$	1.32	1.20	<u>0.0036</u>
$R_{90}/R_{50}$	2.2	2.3	0.2320
$R_e$	2	1	<u>0.0002</u>

NOTE.—Columns: (1) properties measured in each sample (all values are medians): absolute magnitude in  $V$  inside  $R_e$ , absolute magnitude in  $I$  inside  $R_e$ , surface brightness in  $V$  at  $R_e$ ,  $V - I$  color at  $R_e$ , concentration index, defined by the ratio of the radii containing 90% and 50% of the Petrosian flux, and effective radius in kiloparsec; (2) and (3) galaxies in HCG and KPG, respectively; (4)  $P$  values from Mann–Whitney test, where underlined values indicate statistically significant differences.

TABLE 10

PROPERTIES OF INTERMEDIATE-TYPE GALAXIES IN DIFFERENT ENVIRONMENTS

Property (1)	HCG (2)	KPG (3)	KIG (4)	HCG-KPG (5)	HCG4-KIG (6)	KPG-KIG (7)
$M_V$	-20.0	-20.1	-20.3	0.3646	0.0631	<u>0.0291</u>
$M_I$	-21.4	-21.3	-21.4	0.4051	0.1983	0.1200
$\mu_{<r_0}$	20.5	20.6	20.4	0.4315	0.2913	0.2470
$\mu_{>r_0}$	22.5	22.5	23.3	0.1697	<u>0.0004</u>	<u>0.0034</u>
$(V-I)_{<r_0}$	1.37	1.30	1.21	0.1368	<u>0.0167</u>	0.1232
$(V-I)_{>r_0}$	1.31	1.26	1.17	0.3642	0.1937	0.2245
$C_{<r_0}$	0.8	0.7	1.2	0.3713	<u>0.0017</u>	<u>0.0032</u>
$C_{>r_0}$	0.8	1.1	1.5	<u>0.0296</u>	<u>0.0132</u>	0.1344
$A_{<r_0}$	1.01	1.01	1.01	0.2415	0.4933	0.2815
$A_{>r_0}$	1.04	1.08	1.06	0.0960	0.3628	0.1300

NOTE.—Columns: (1) properties measured in each sample (all values are medians): absolute magnitude in  $V$  inside  $r_0$ , absolute magnitude in  $I$  inside  $r_0$ , surface brightness in  $V$  inside and outside  $r_0$ ,  $V-I$  color inside and outside  $r_0$ , concentration index inside and outside  $r_0$ , asymmetry level inside and outside  $r_0$ ; (2)–(4) galaxies in HCG, KPG, and KIG, respectively; (5)–(7)  $P$  values from Dunn’s post-tests, where underlined values indicate statistically significant differences.

TABLE 11

MEDIAN VALUES OF INTERMEDIATE-TYPE GALAXIES AS MEASURED USING  $R_e$   $R_e$ 

Property (1)	HCG (2)	KPG (3)	KIG (4)	HCG-KPG (5)	HCG-KIG (6)	KPG-KIG (7)
$M_V$	-20.7	-20.5	-20.3	0.2536	0.2375	0.5000
$M_I$	-21.7	-21.7	-21.4	0.3837	0.1465	0.2848
$\mu_V$	21.1	20.9	20.5	0.1445	<u>0.0054</u>	0.0511
$(V-I)$	1.23	1.17	1.09	0.3083	0.0517	0.1417
$R_{90}/R_{50}$	2.1	2.1	2.2	0.0714	0.1363	<u>0.0156</u>
$R_e$	4	4	3	0.2367	<u>0.0059</u>	0.0863

NOTE.—Columns: (1) properties measured in each sample (all values are medians): absolute magnitude in  $V$  inside  $R_e$ , absolute magnitude in  $I$  inside  $R_e$ , surface brightness in  $V$  at  $R_e$ ,  $V-I$  color at  $R_e$ , concentration index, defined by the ratio of the radii containing 90% and 50% of the Petrosian flux, and effective radius in kiloparsec; (2)–(4) galaxies in HCG, KPG, and KIG, respectively; (5)–(7)  $P$  values from Dunn’s post-tests. Underlined values indicate statistically significant differences.

TABLE 12

PROPERTIES OF LATE-TYPE GALAXIES IN DIFFERENT ENVIRONMENTS

Property (1)	HCGs (2)	KPGs (3)	KIGs (4)	HCG-KPG (5)	HCG-KIG (6)	KPG-KIG (7)
$M_V$	-19.1	-19.2	-19.4	0.2265	<u>0.0290</u>	0.1657
$M_I$	-20.3	-20.7	-20.8	0.3303	0.0560	0.1797
$\mu_{<r_0}$	21.2	20.9	21.0	<u>0.0250</u>	0.1530	0.1758
$\mu_{>r_0}$	22.4	22.6	22.7	0.2172	0.2961	0.4617
$(V-I)_{<r_0}$	1.27	1.26	1.30	0.3723	0.3455	0.1833
$(V-I)_{>r_0}$	1.27	1.15	1.30	0.4493	0.1280	0.0794
$C_{<r_0}$	0.6	0.7	0.6	0.2092	0.4323	0.1943
$C_{>r_0}$	0.7	0.9	0.8	0.0963	<u>0.0123</u>	0.2601
$A_{<r_0}$	1.03	1.02	1.01	0.3392	<u>0.0007</u>	<u>0.0019</u>
$A_{>r_0}$	1.09	1.15	1.08	0.0801	0.1400	<u>0.0004</u>

NOTE.—ines and columns are the same as defined in Table 7

TABLE 13  
 PROPERTIES OF LATE-TYPE GALAXIES AS MEASURED USING  $R_e$

Property (1)	HCG (2)	KPG (3)	KIG (4)	HCG-KPG (5)	HCG-KIG (6)	KPG-KIG (7)
$M_V$	-20.4	-19.9	-20.8	0.0707	0.0793	<u>0.0030</u>
$M_I$	-21.7	-21.0	-21.9	0.0960	0.1988	<u>0.0035</u>
$\mu_V$	21.4	21.5	21.6	0.4866	0.2081	<u>0.0890</u>
$(V - I)$	1.25	1.03	1.12	<u>0.0156</u>	0.1021	0.0715
$R_{90}/R_{50}$	1.9	1.8	1.8	0.3304	0.0996	0.1170
$R_e$	5	3	5	0.0802	0.1448	<u>0.0064</u>

NOTE.—ines and columns are the same as defined in Table 12

## REFERENCES

- Abraham, R. G., Tanvir, N. R., Santiago, B. X., Ellis, R. S., Glazebrook, K., & van den Bergh, S. 1996, *MNRAS*, 279, L47
- Abraham, R. G., Valdes, F., Yee, H. K. C., & van den Bergh, S. 1994, *ApJ*, 432, 75
- Barnes, J. E. 1996, in *IAU Symp. 171, New Light on Galaxy Evolution*, ed. Bender, R., & Davies, L. (Dordrecht: Kluwer), 191
- Barth, C. S., Coziol, R., & Demers, S. 1995, *MNRAS*, 276, 1224
- Bender, R.; Döbereiner, S., & Möllenhoff, C., 1988, *A&AS*, 74, 385
- Bender, R., & Möllenhoff, C. 1987, *A&A*, 177, 71
- Blackburn, J. K. 1995, in *ASP Conf. Ser., 77, Astronomical Data Analysis Software and Systems IV*, ed. Shaw, R. A.; Payne, H. E., & Hayes, J. J. E. (San Francisco, CA: ASP), 367
- Conselice, C. J. 1997, *PASP*, 109, 1251
- Conselice, C. J., Bershady, M. A., & Jangren, A. 2000, *ApJ*, 529, 886
- Coziol, R. 2003, *MNRAS*, 344, 181
- Coziol, R., Brinks, E., & Bravo-Alfaro, H. 2004, *AJ*, 128, 68
- Coziol, R., & Plauchu-Frayn, I. 2007, *AJ*, 133, 2630
- Graham, A. W, Driver, S. R., Petrosian, V., Conselice, C. J., Bershady, M.A., Crawford, S. M., & Goto, T. 2005, *AJ*, 130, 1535
- Hernández-Toledo, H. M., Dultzin-Hacyan, D., González, J. J., & Sulentic, J.W. 1999, *AJ*, 118, 108
- Hernquist, L. 1993, *ApJ*, 409, 548
- Hickson, P. 1982, *ApJ*, 255, 382
- Hickson, P., Mendes de Oliveira, C., Huchra, J. P., & Palumbo, G. G. 1992 *ApJ*, 399, 353
- Hutchings, J. B., & Proulx, C. 2008, *AJ*, 135, 1692
- Jedrzejewski, R. I., 1987, *MNRAS*, 226, 747
- Karachentsev, I. D. 1987, *Double Galaxies* (translated by W. Keel, University of Alabama, and N. Sharp, National Optical Astronomy Observatories from Moscow, Izdatel'stvo Nauka and published on webpage: <http://nedwww.ipac.caltech.edu/level5/Sept02/Keel/frames.html>)
- Karachentsev, I. D. 1972, *Soobshch. Spec. Astrop. Obs.*, 7, 1
- Karachentseva, V. E. 1973, *Soobshch. Spec. Astrop. Obs.*, 8, 3
- Kormendy, J. 1982 in *Proc. 12th Advanced Course (A84-15502 04-90), Morphology and Dynamics of Galaxies* (Sauverny: Observatoire de Geneve) 113
- Landolt, A. U., 1992, *AJ*, 104, 340
- Makino, J., & Hut, P. 1997, *ApJ*, 481, 83
- Mendes de Oliveira, C., & Hickson, P. 1994, *ApJ*, 427, 684
- Naab T., & Burkert A., 2003, *ApJ*, 597, 893
- Nieto, J.-L. Bender, R., Poulain, P., & Surma, P. 1992, *A&A*, 257, 97
- Patton, D. R., Carlberg, R. G., Marzke, R. O., Pritchet, C. J., da Costa, L. N., & Pellegrini, P. S. 2000, *ApJ*, 536, 153
- Paturel, G., Petit, C., Prugniel, P., Theureau, G., Rousseau, J., Brouty, M., Dubois, P., & Cambrésy, L., 2003, *A&A*, 412, 45
- Petrosian, V. 1976, *ApJ*, 209, L1
- Plauchu-Frayn, I., & Coziol, R. 2010, *AJ*, submitted
- Ribas, I., Jordi, C., Vilardell, F., & Fitzpatrick, E. L. *Letter* 2005, *ApJ*, 635, 37
- Schade, D., Lilly, S. J., Crampton, D., Hammer, F., Le Fevre, O., & Tresse, L. 1995, *ApJ*, 451, 1
- Schlegel, D. J., Finkbeiner, D. P., & Davis, M., 1998, *ApJ*, 500, 525
- Schuster, W. J., & Parrao, L., 2001, *RevMexAA*, 37, 187
- Shimasaku, K., et al. 2001, *AJ*, 122, 1238

- Sulentic, J. W., et al. 2006, *A&A*, 449, 937
- Tully, R. B. 1987, *ApJ*, 321, 280
- Turner, E. L. 1976, *ApJ*, 208, 304
- Turner, E. L., Aarseth, S. J., Blanchard, N. T.,  
Mathieu, R. D., & Gott, J. R., III 1979, *AJ*,  
228, 684
- van Dokkum, P. G. 2005, *AJ*, 130, 2647
- Vettolani, G., de Souza, R., & Chincarini, G. 1986,  
*A&A*, 154, 343
- Zaritsky, D., & Lo, K. Y., 1986, *ApJ*, 303, 66
- Zwicky, F., Herzog, E., Wild, P., Karpowicz, M.,  
& Kowal, C 1961-1968 *Catalog of Galaxies and  
Clusters of Galaxies*, in 6 vols. (Pasadena, CA:  
California Institute of Technology) (CGCG)

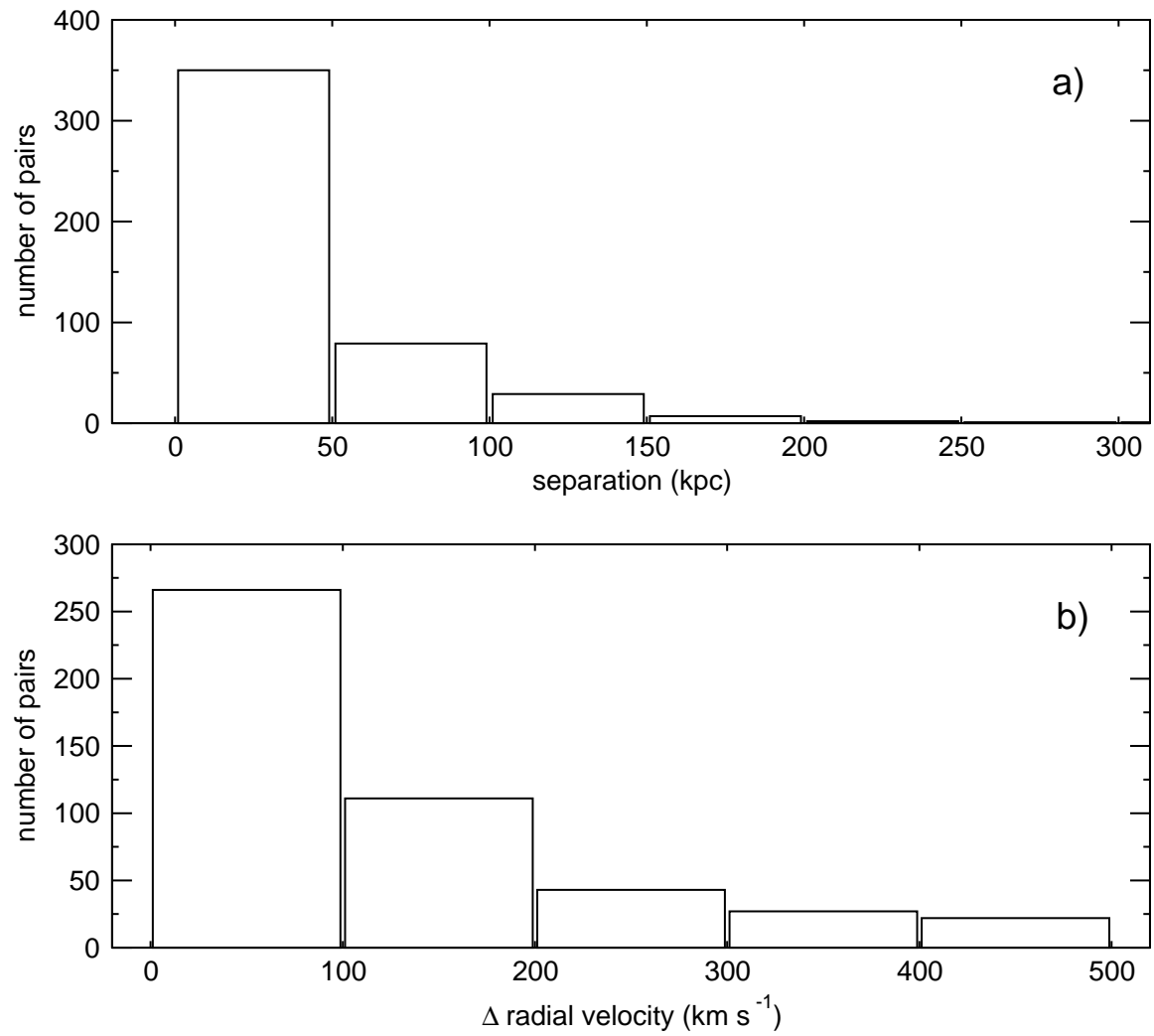


Fig. 1.— Distribution of pairs as a function of (a) linear separation and (b) difference in radial velocity of the pair members.

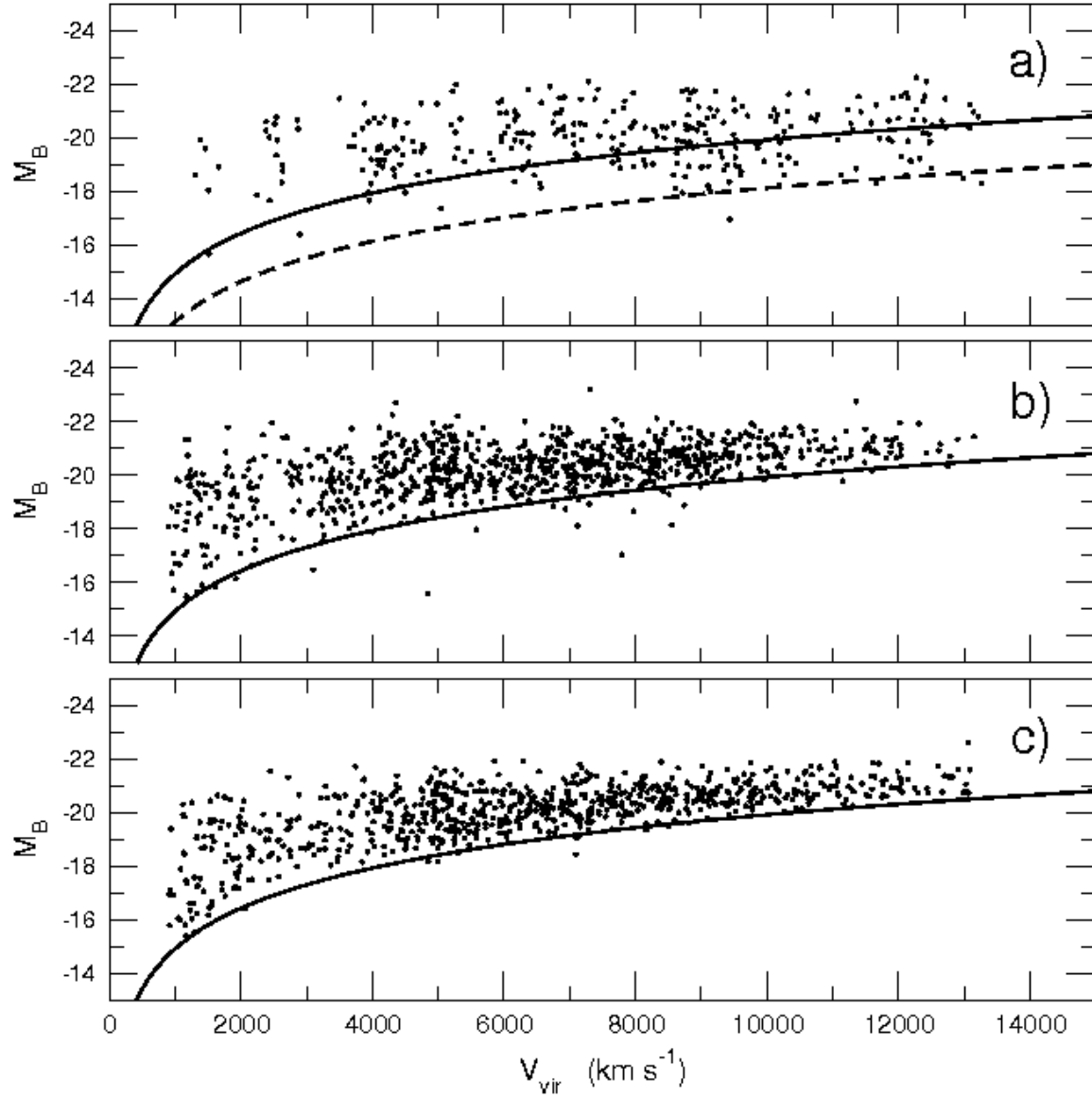


Fig. 2.— Distribution of absolute  $B$  magnitude vs. virgocentric velocity for (a) HCG, (b) KPG, (c) and KIG. The curves indicate the magnitude limit of the survey for the HCG catalog  $m_B=17.5$  (*dashed curve*) and the KPG and KIG catalogs  $m_B=15.7$  (*continuous curve*). The data have been extracted from HyperLEDA.

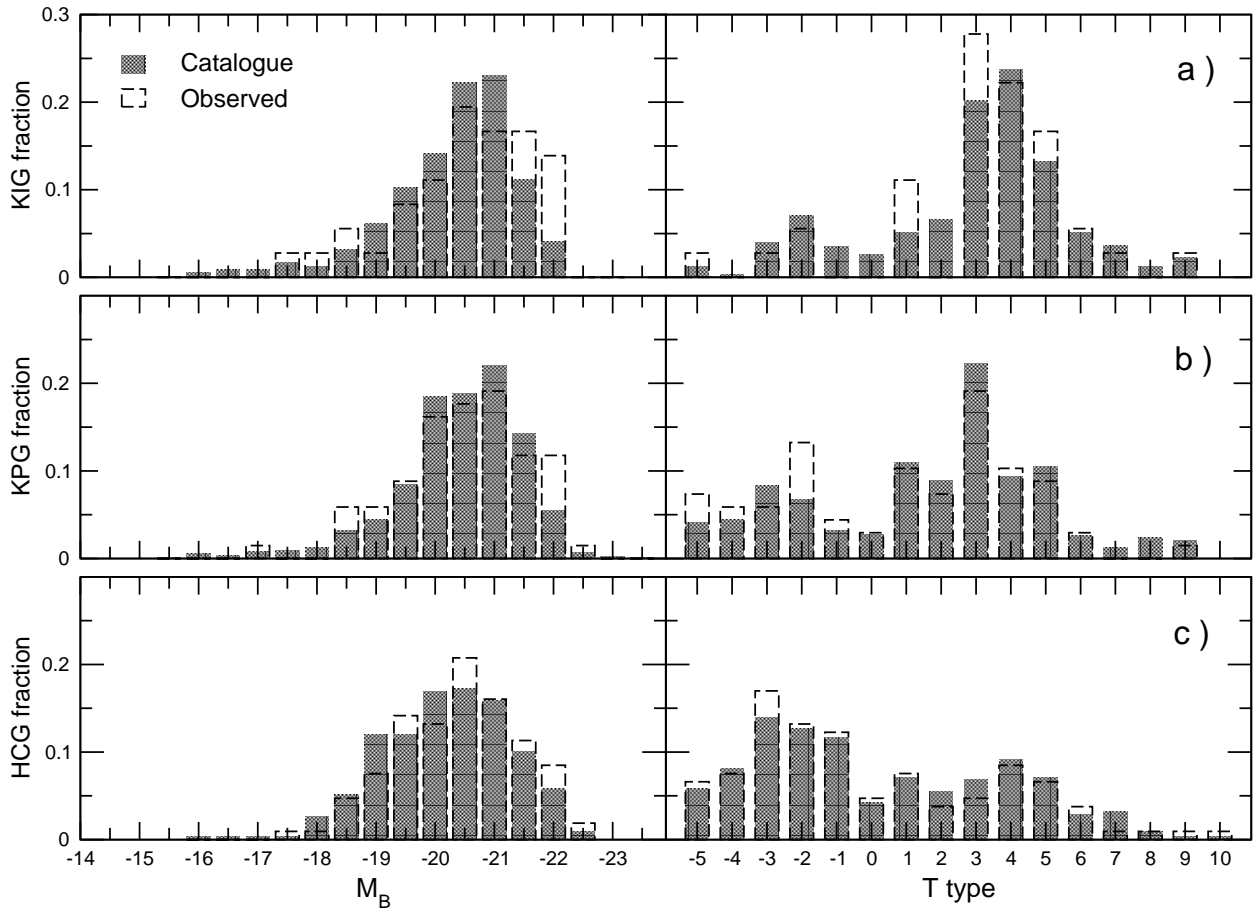


Fig. 3.— Distribution of catalog vs. observed galaxies (a) KIGs, (b) KPGs, and (c) HCGs.

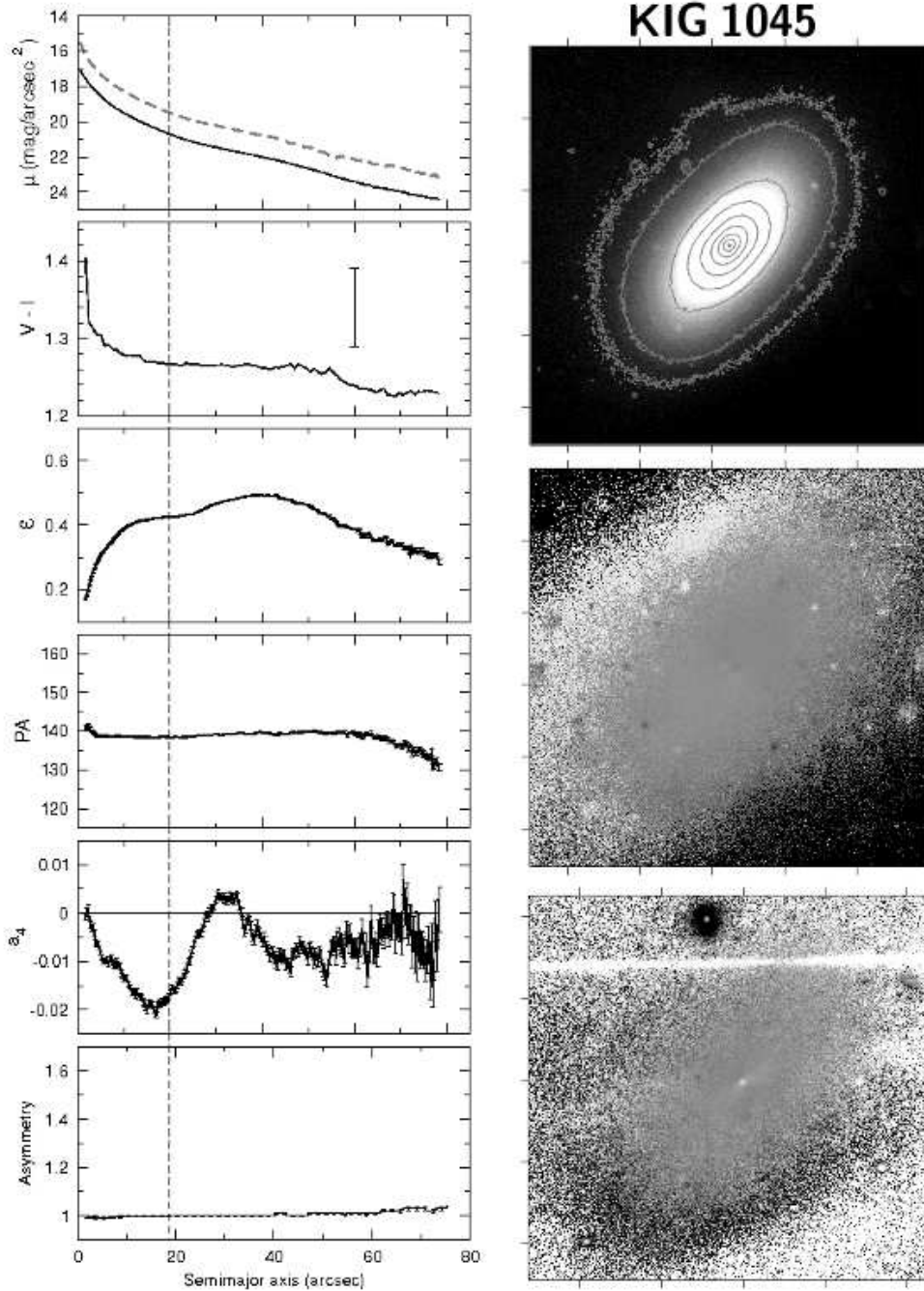


Fig. 4.— KIG 1045 mosaic. Left panel: isophotal parameter profiles as a function of semi-major axis  $a$ —from top to bottom: surface brightness  $V$  (solid curve) and  $I$  (dashed curve),  $V - I$  index color, ellipticity, P.A., isophotal deviation from pure ellipse, and asymmetry level. The dashed vertical line indicates the average half-radius  $r_0 = 5$  kpc (or  $r_0 = 2.5$  kpc when indicated). Right panel:  $V$ -band image, displayed on a logarithmic scale with superimposed isophotes; the residual image (middle right) and the  $V - I$  color map (bottom image). North is up and east is to the left. (The complete figure set (214 images) is available in the online journal.)

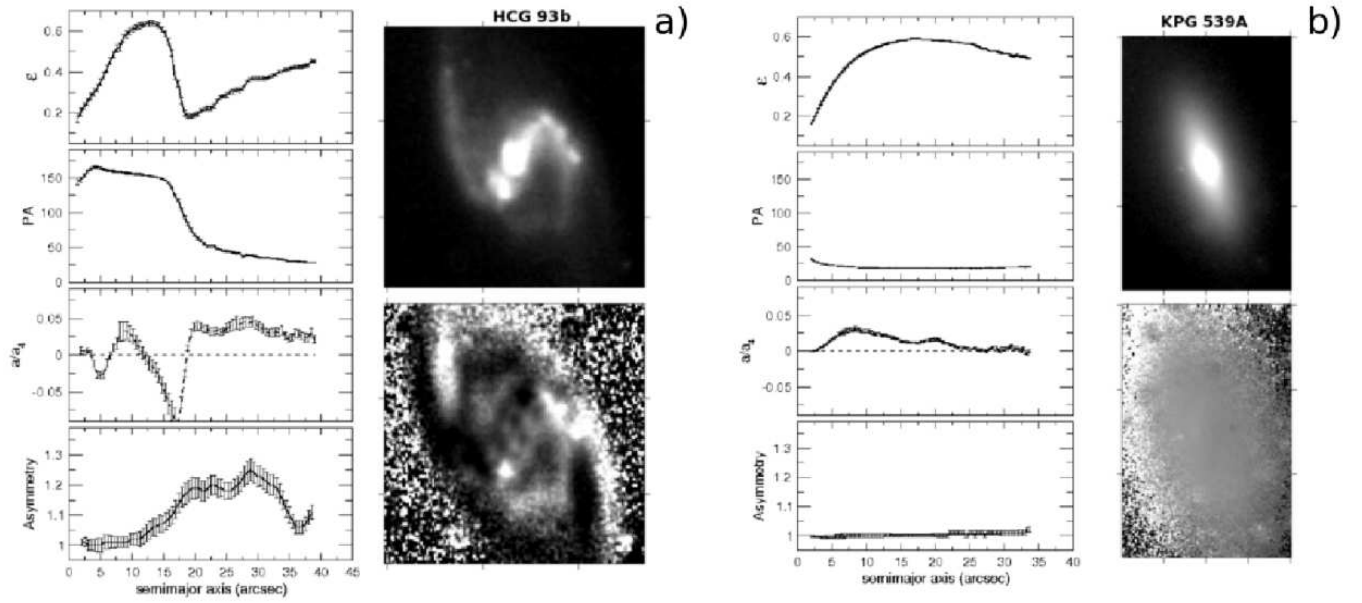


Fig. 5.— Isophotal and asymmetry profiles (a) the asymmetric galaxy, HCG 93b and (b) the symmetric galaxy KPG 539A. The images show that both methods (isophotal and asymmetry) are complementary: variations in isophotal parameters follow variation in asymmetry and vice versa.

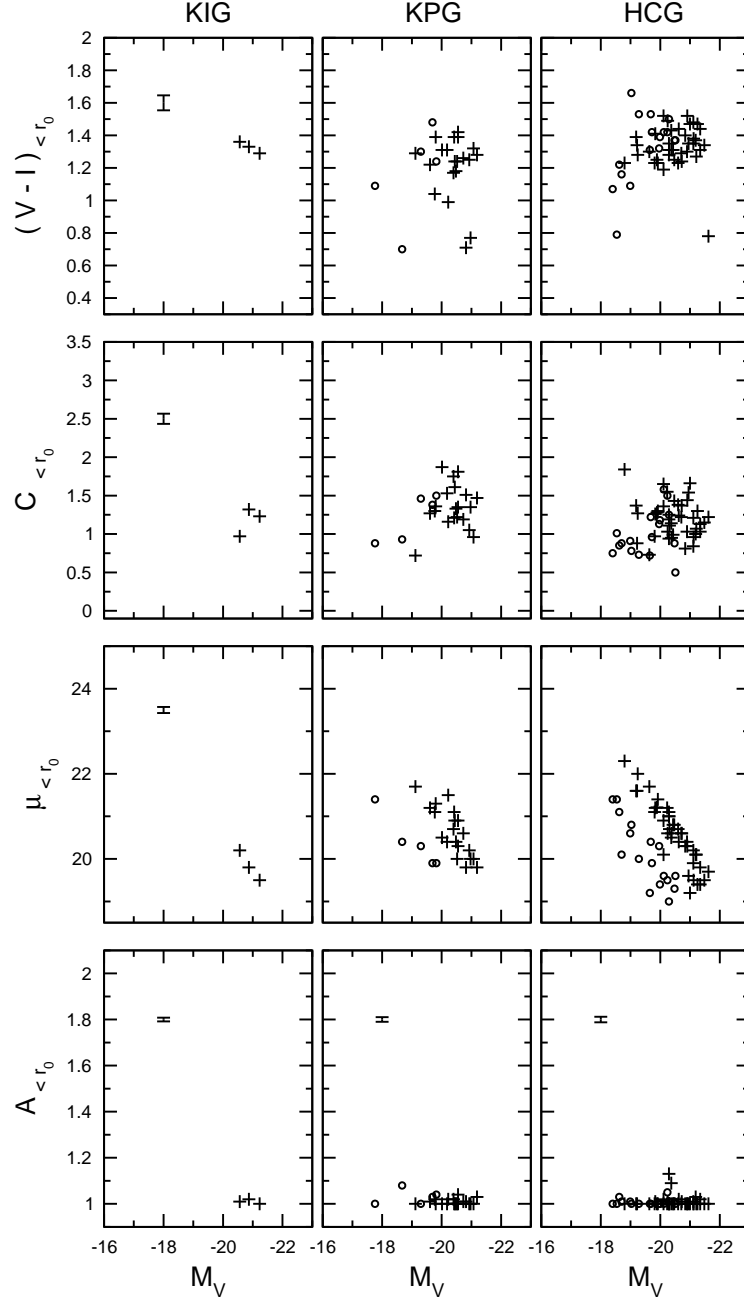


Fig. 6.— Variations in early-type galaxies of isophotal parameters and asymmetry as a function of absolute magnitude in  $V$  inside  $r_0$  for —from left to right: —KIG, KPG, and HCG early-type galaxies. The parameter values are measured inside the average half-radius  $r_0 = 5$  kpc. For smaller size galaxies (open circle), the average half-radius is  $r_0 = 2.5$  kpc.

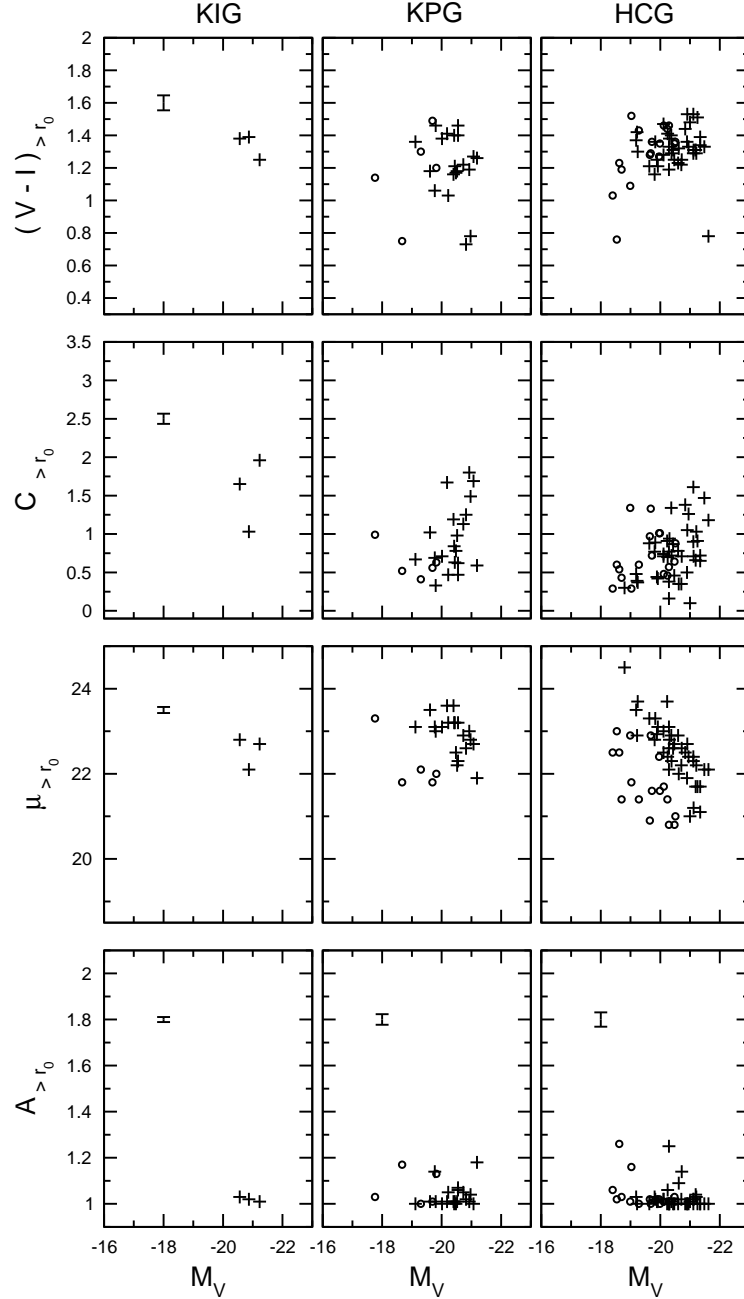


Fig. 7.— Variations in early-type galaxies of isophotal parameters and asymmetry as a function of absolute magnitude in  $V$  inside  $r_0$  for —from left to right: —KIG, KPG, and HCG early-type galaxies. The parameters are measured outside the average half-radius  $r_0 = 5$  kpc. For smaller size galaxies (open circle), the average half-radius is  $r_0 = 2.5$  kpc.

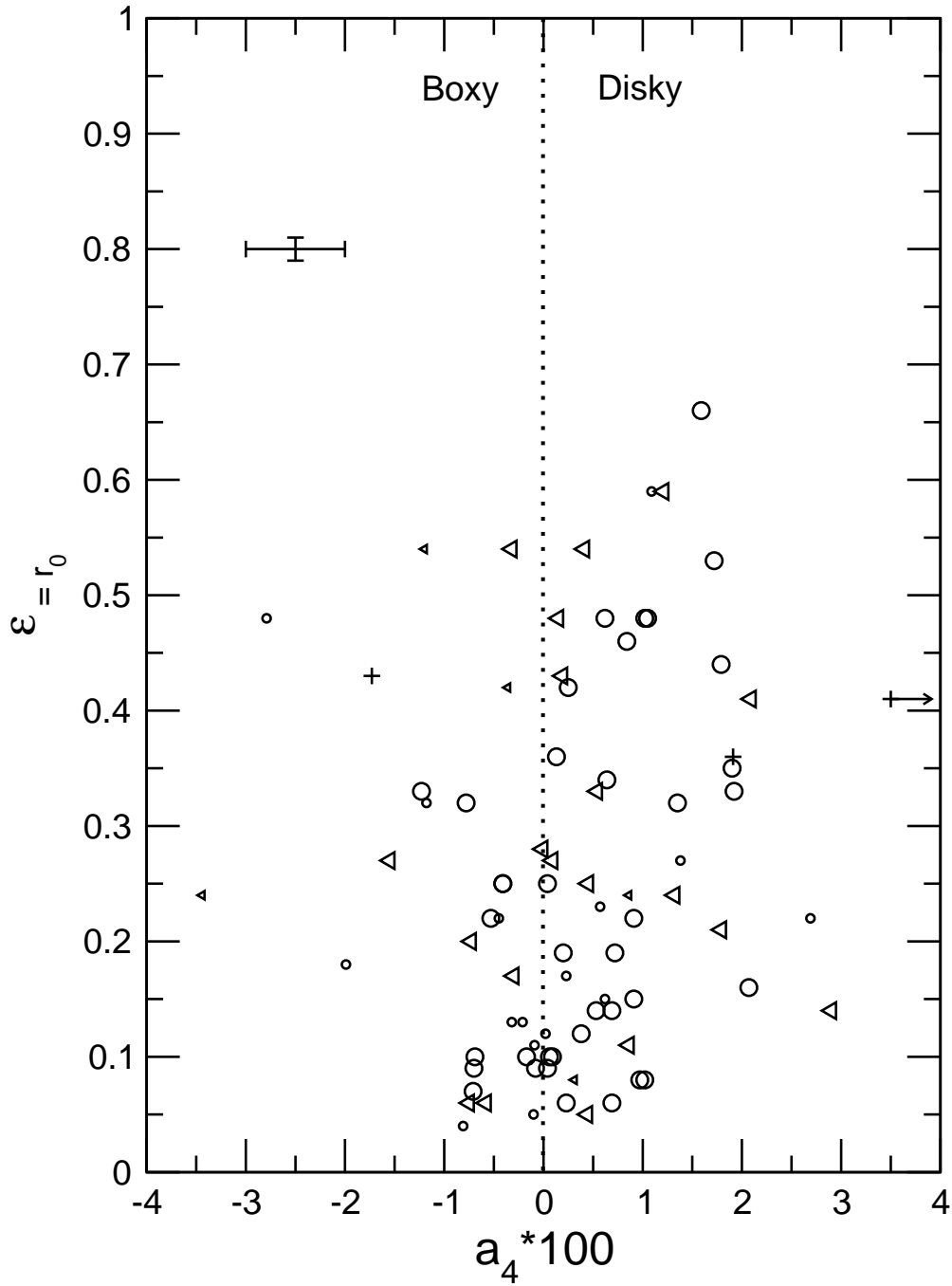


Fig. 8.— Isophotal shape as based on the  $a_4$  parameter vs. ellipticity,  $\epsilon$ , for early-type galaxies. Both values were measured at  $r_0$ . Symbols correspond to HCG (open circles), KPG (triangles), and KIG (plus signs) galaxies. Smaller symbols correspond to small size galaxies (with  $r_0 = 2.5$  kpc).

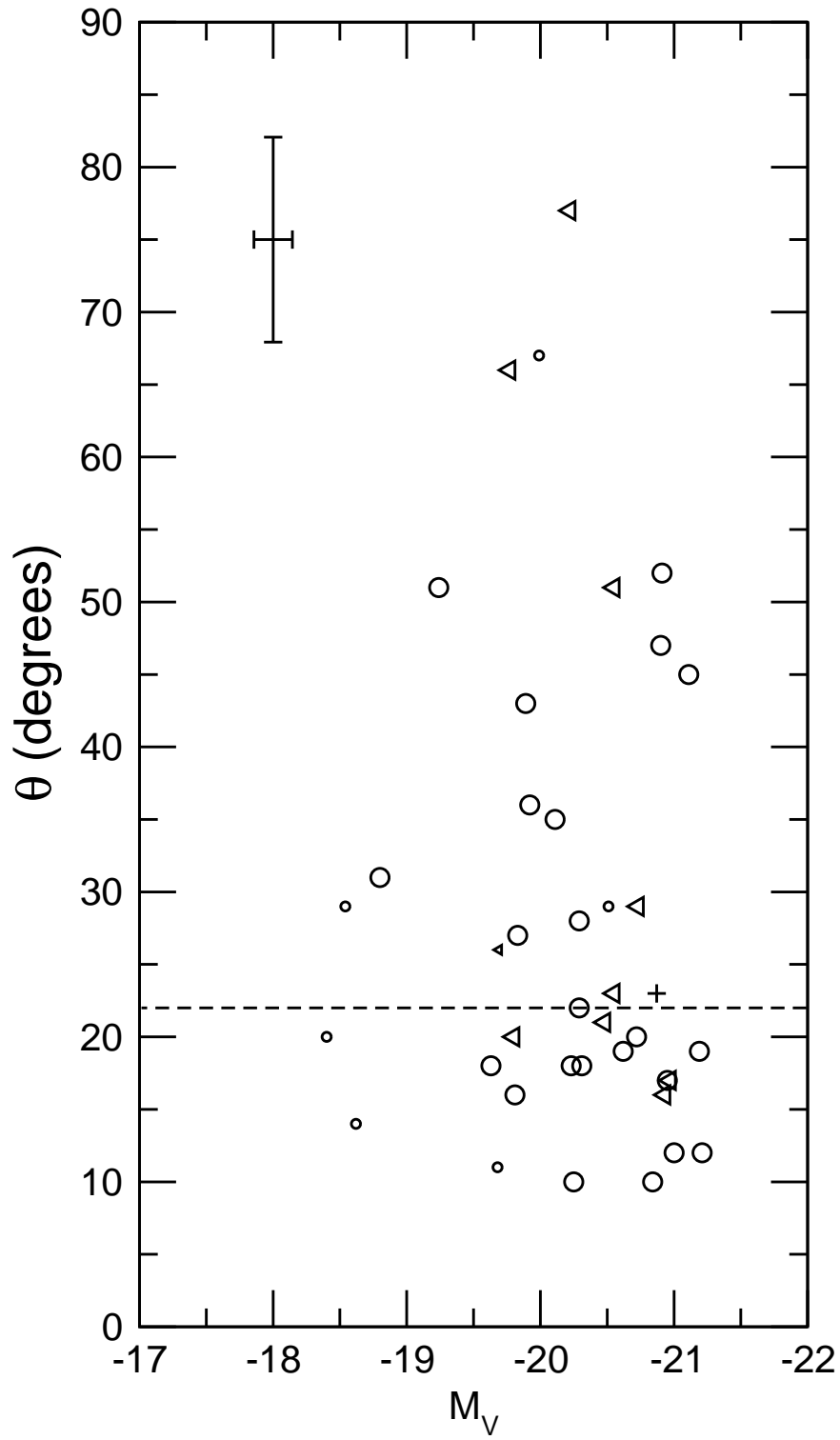


Fig. 9.— Early-type galaxies with high twists,  $\theta$ , as a function of absolute magnitude in  $V$ . Symbols are the same as in Figure 8.

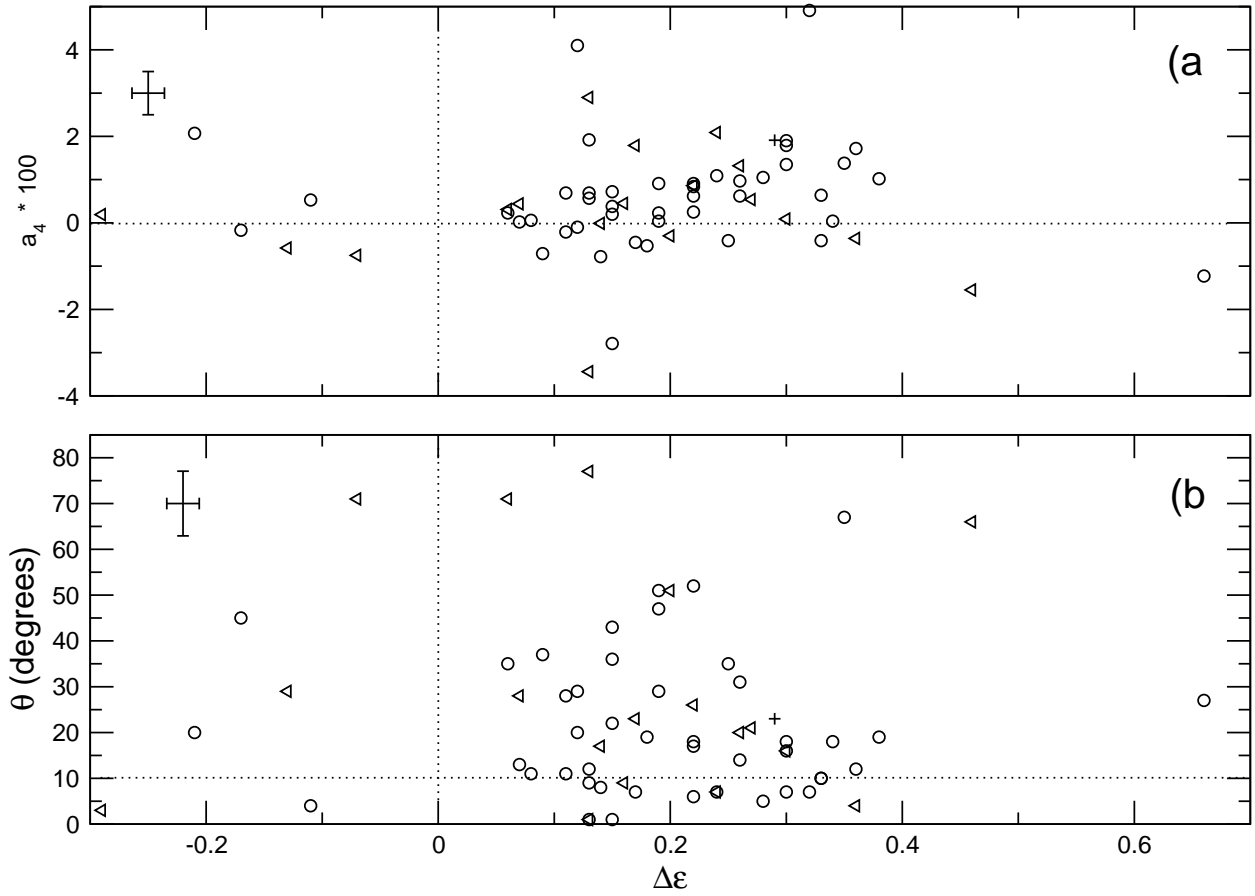


Fig. 10.— Ellipticity variation,  $\Delta\epsilon$  vs. (a) isophotal shape  $a_4$  and (b) twist  $\theta$  for E-S0 galaxies: HCGs (open circles), KPGs (open triangles), and KIGs (plus signs).

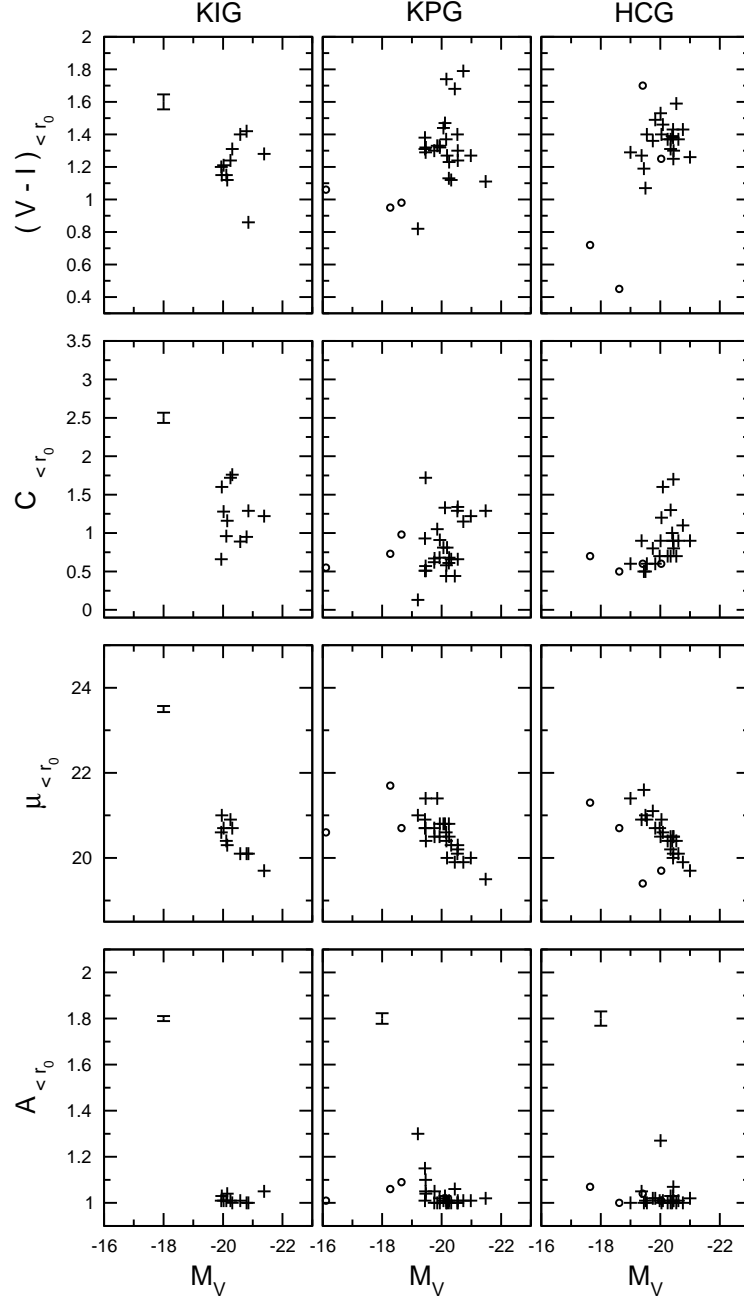


Fig. 11.— Variations in intermediate-type galaxies of isophotal parameters and asymmetry as a function of absolute magnitude in  $V$  inside  $r_0$  for —from left to right—KIG, KPG, and HCG intermediate-type galaxies. The parameters are measured inside the average half-radius  $r_0 = 5$  kpc. For smaller size galaxies (open circle), the average half-radius is  $r_0 = 2.5$  kpc.

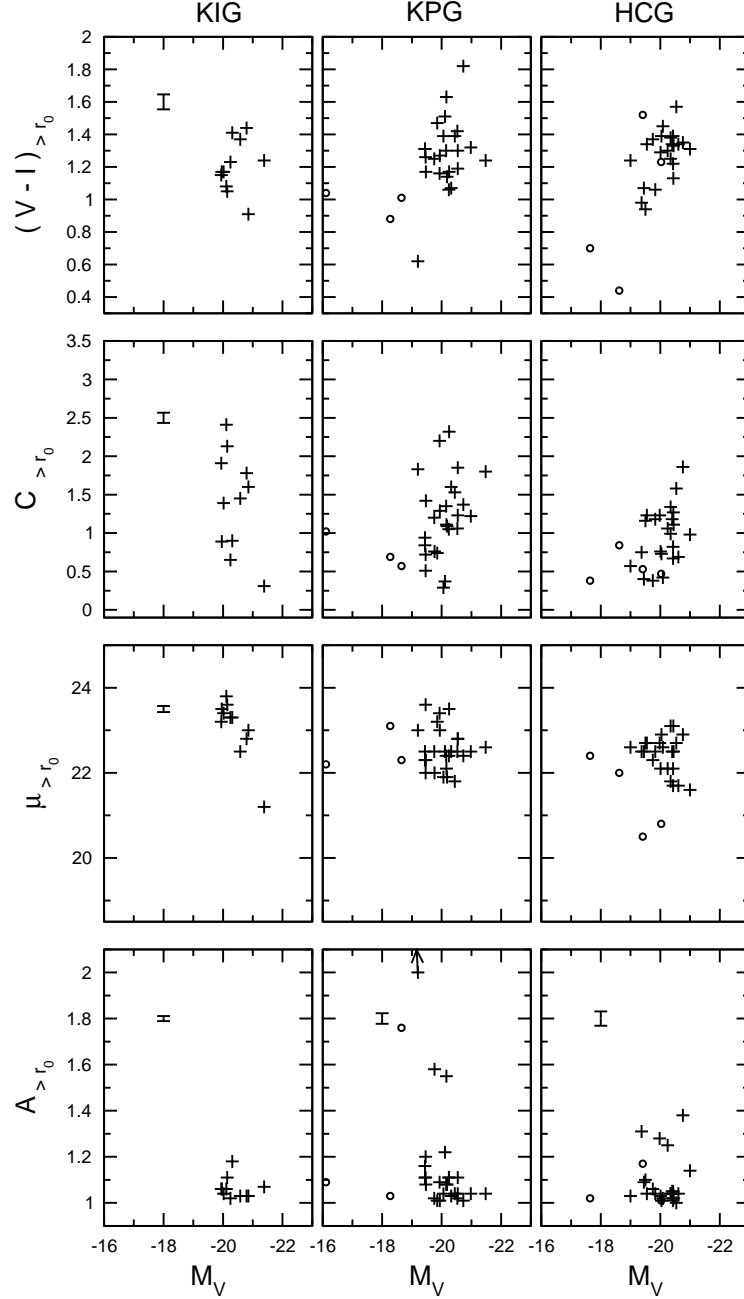


Fig. 12.— Variations in intermediate-type galaxies of isophotal parameters and asymmetry as a function of absolute magnitude in  $V$  inside  $r_0$  for —from left to right —KIG, KPG, and HCG intermediate-type galaxies. The parameters are measured outside the average half-radius  $r_0 = 5$  kpc. For smaller size galaxies (open circle), the average half-radius is  $r_0 = 2.5$  kpc.

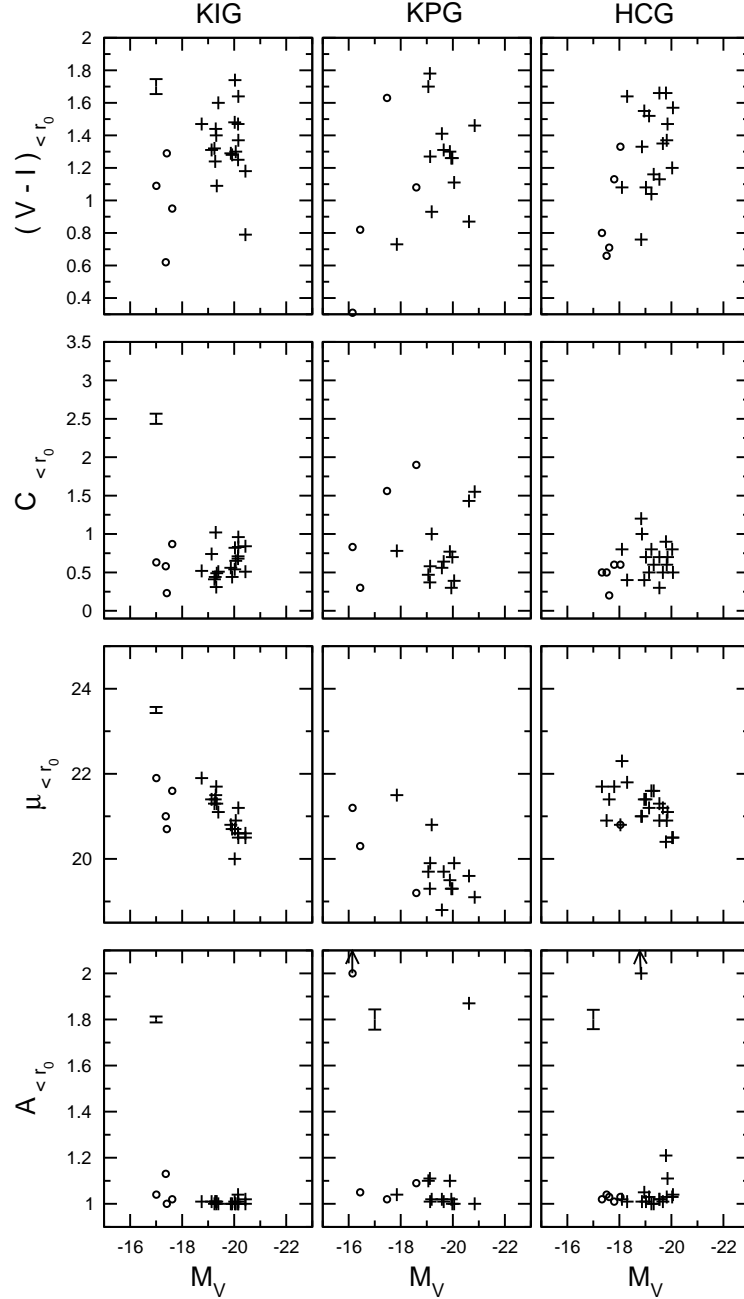


Fig. 13.— Variations in late-type galaxies of isophotal parameters and asymmetry as a function of absolute magnitude in  $V$  inside  $r_0$  for —from left to right— KIG, KPG, and HCG late-type galaxies. The parameters are measured inside the average half-radius  $r_0 = 5$  kpc. For smaller size galaxies (open circle), the average half-radius is  $r_0 = 2.5$  kpc.

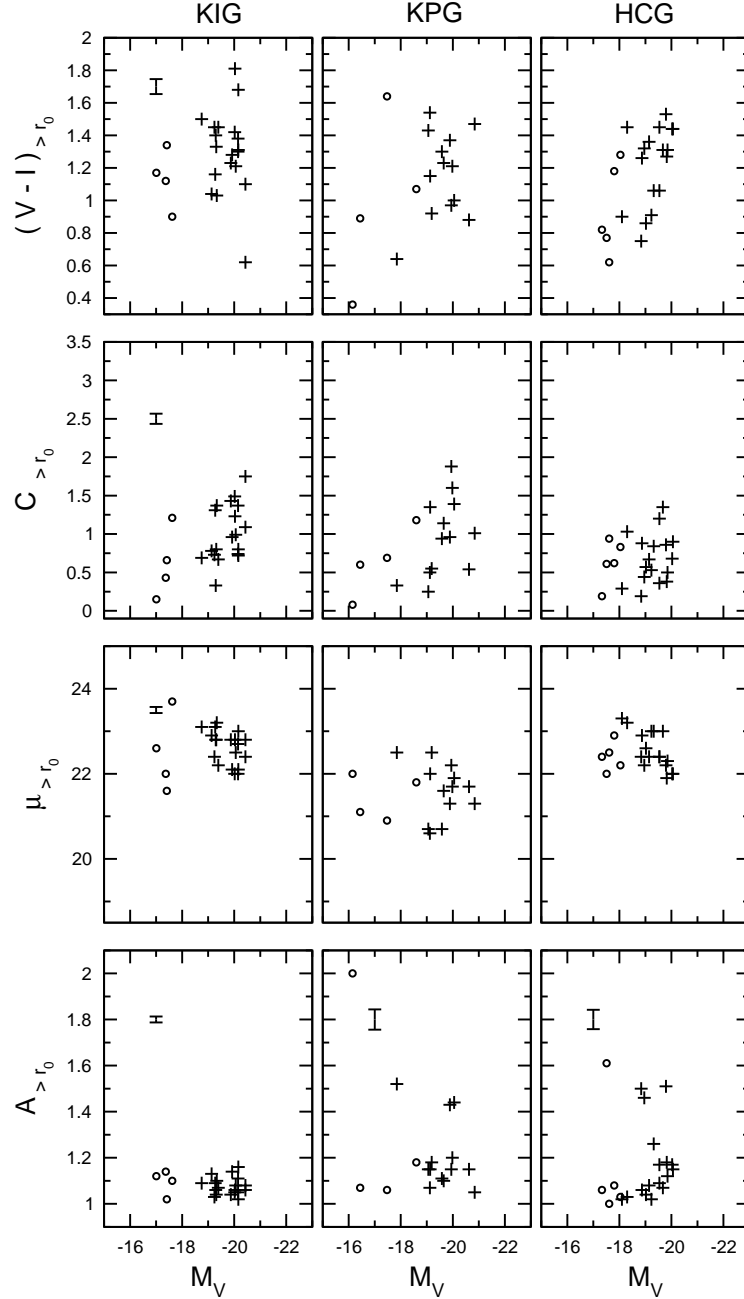


Fig. 14.— Variations in late-type galaxies of isophotal parameters and asymmetry as a function of absolute magnitude in  $V$  inside  $r_0$  for —from left to right— KIG, KPG, and HCG late-type galaxies. The parameters are measured outside the average half-radius  $r_0 = 5$  kpc. For smaller size galaxies (open circle), the average half-radius is  $r_0 = 2.5$  kpc.

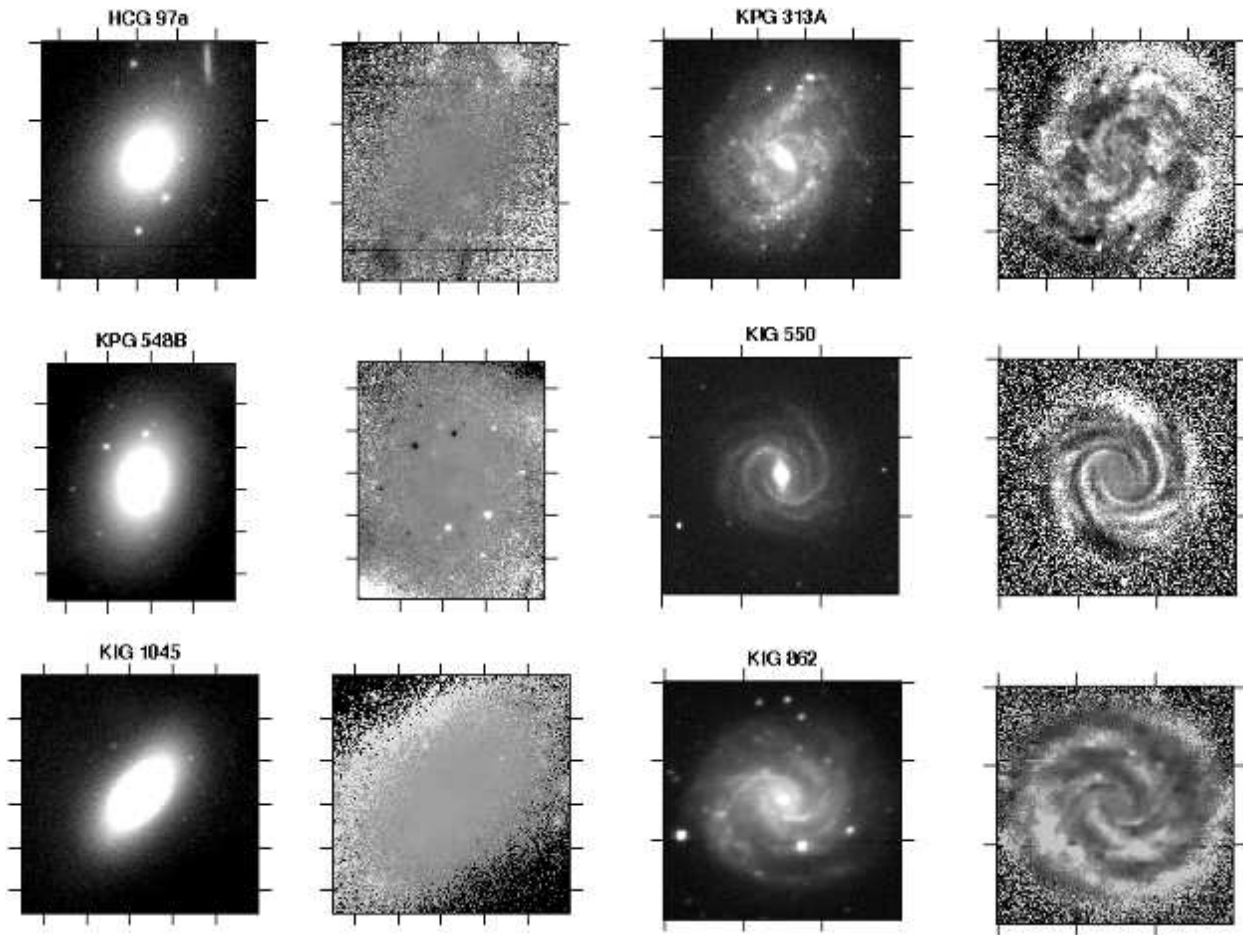


Fig. 15.— Examples of type 1 asymmetries Left: symmetric galaxies; right: galaxies where the asymmetries are intrinsic, related to star formation regions and/or spiral arm structures. The  $V$  images are displayed in logarithmic scales together with their residual images.

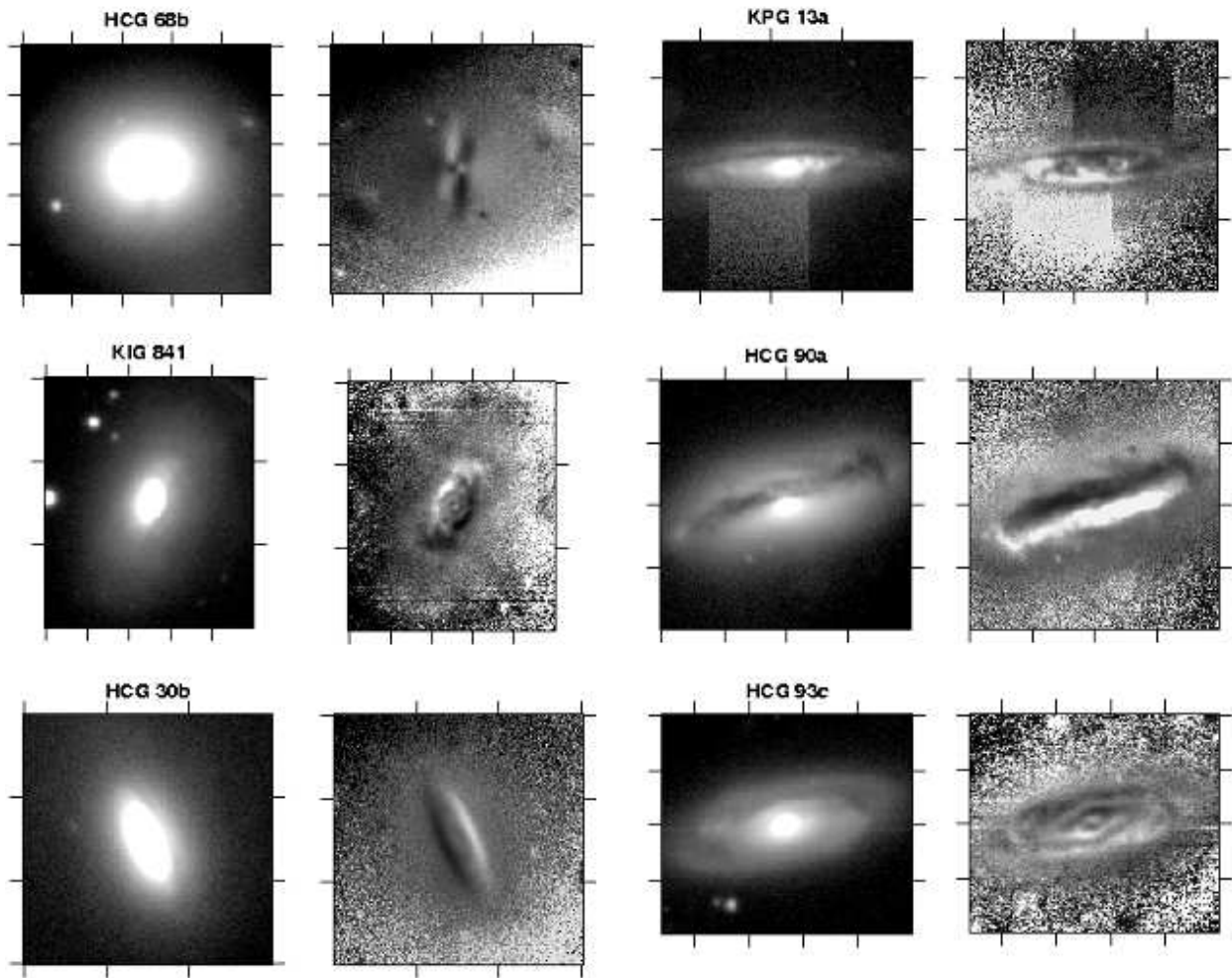


Fig. 16.— Examples of type 2 asymmetries: asymmetry is related to dust lanes in the disk and/or due to the inclination of the disk on the sky. The images are displayed in the same way as in Figure 15.

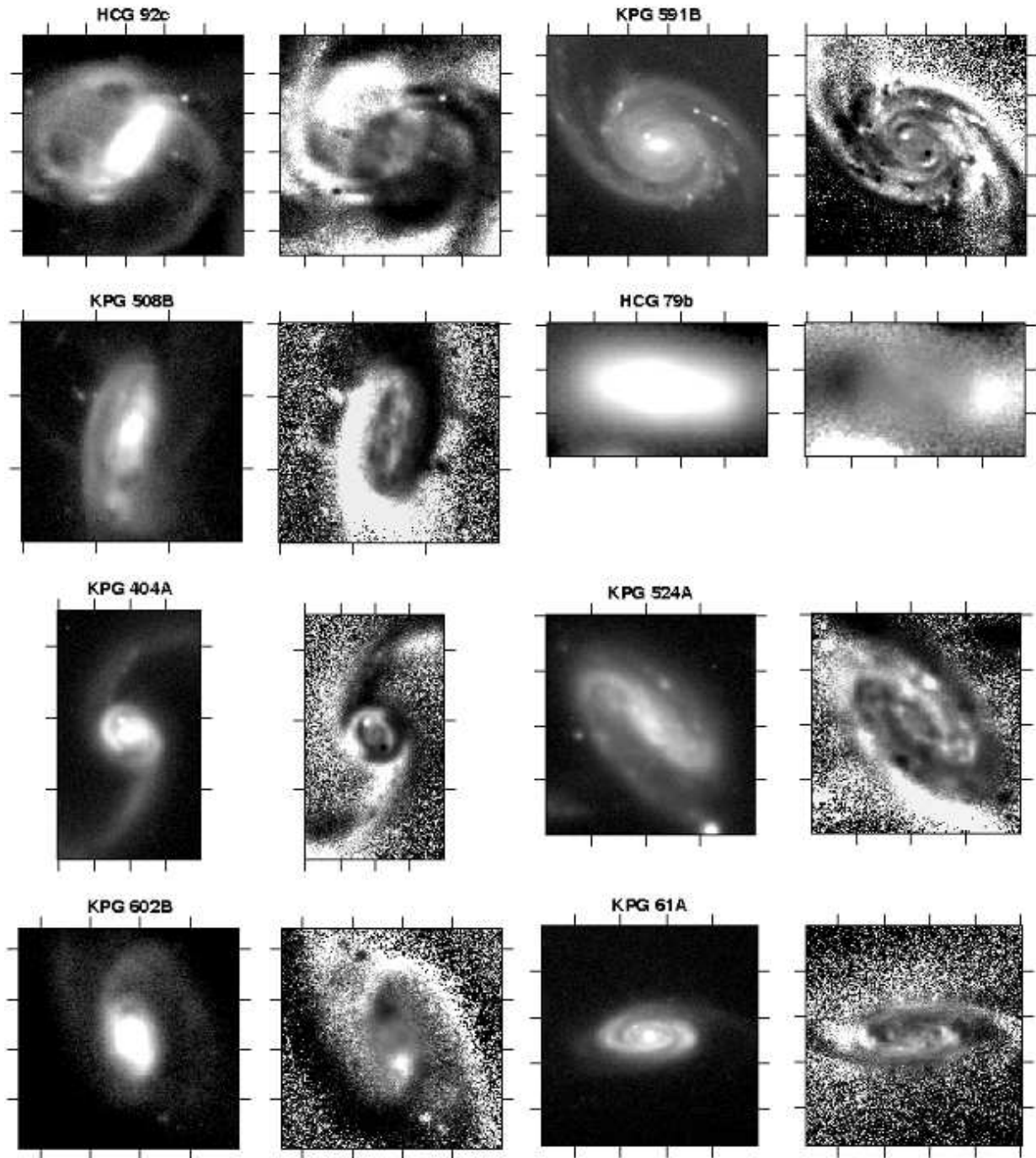


Fig. 17.— Examples of type 3 asymmetries. These are obvious cases of asymmetries related to galaxies interactions. The images are displayed in the same way as in Figure 15.

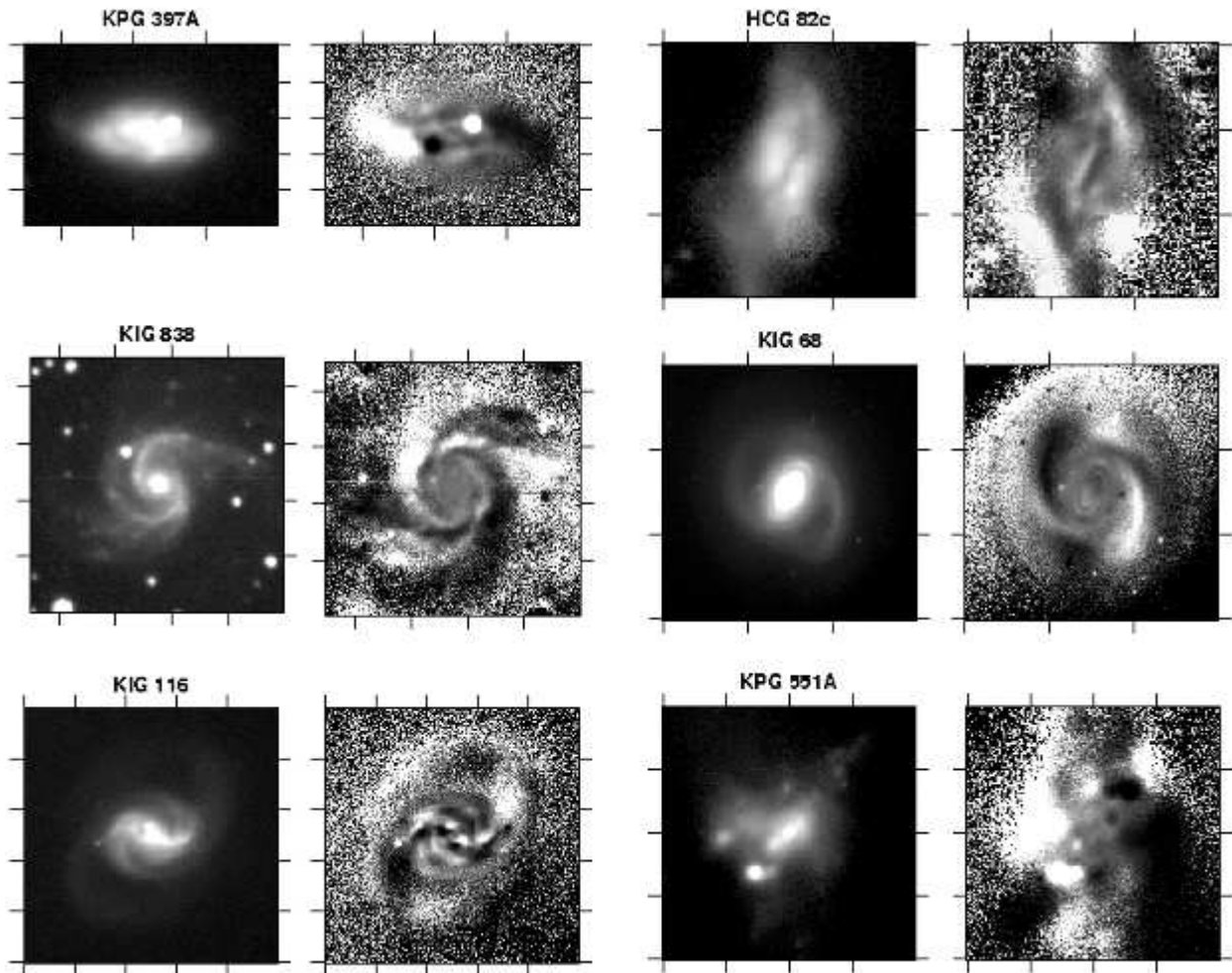


Fig. 18.— Examples of type 4 asymmetries. Asymmetric structures appear, but their cause is not obvious. The images are displayed in the same way as in Figure 15.

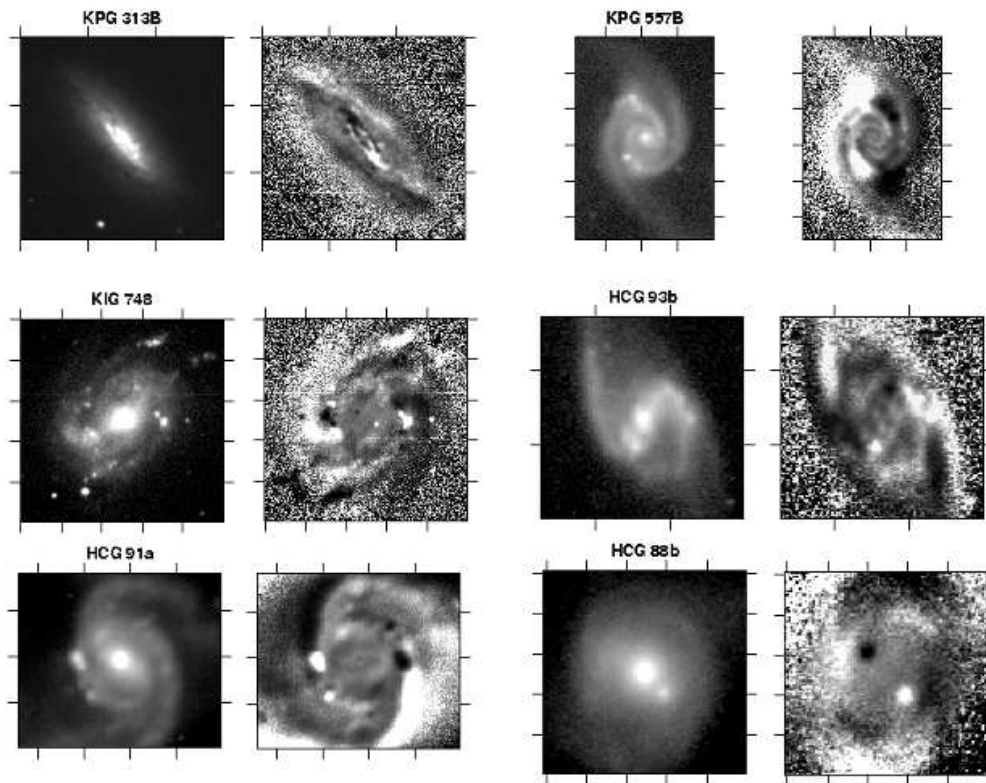


Fig. 19.— Examples of type 5 asymmetries. A companion galaxy appears near the center. The images are displayed in the same way as in Figure 15.

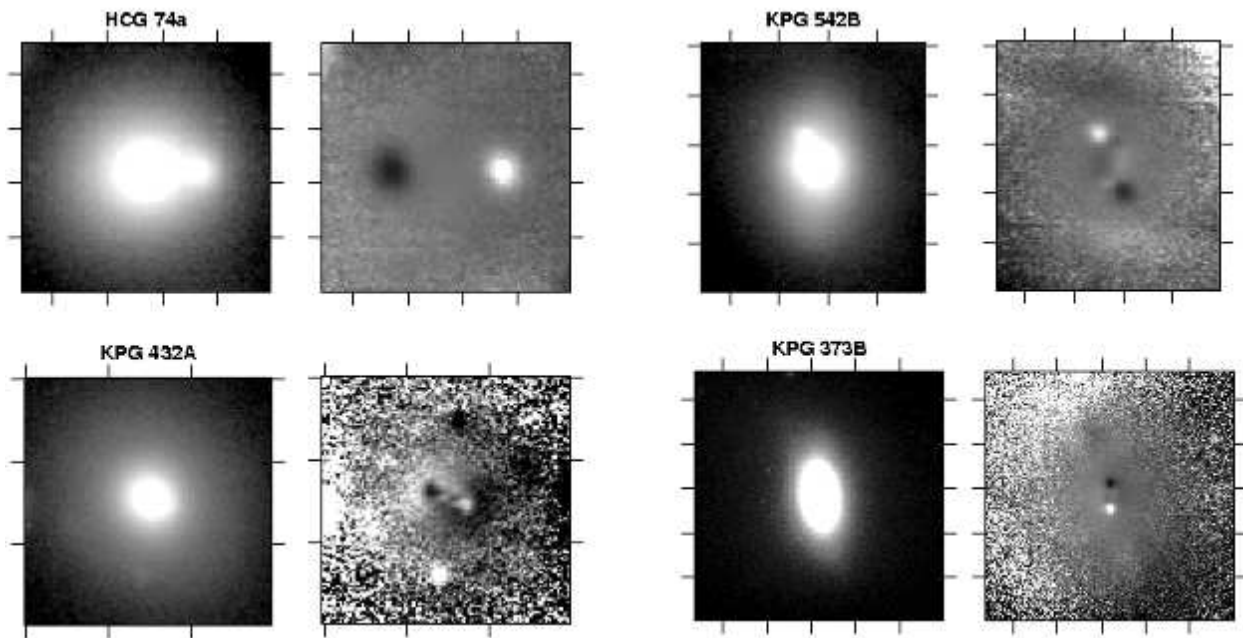


Fig. 20.— Examples of type 6 asymmetries. A possible double nucleus is observed in these images. The images are displayed in the same way as in Figure 15.

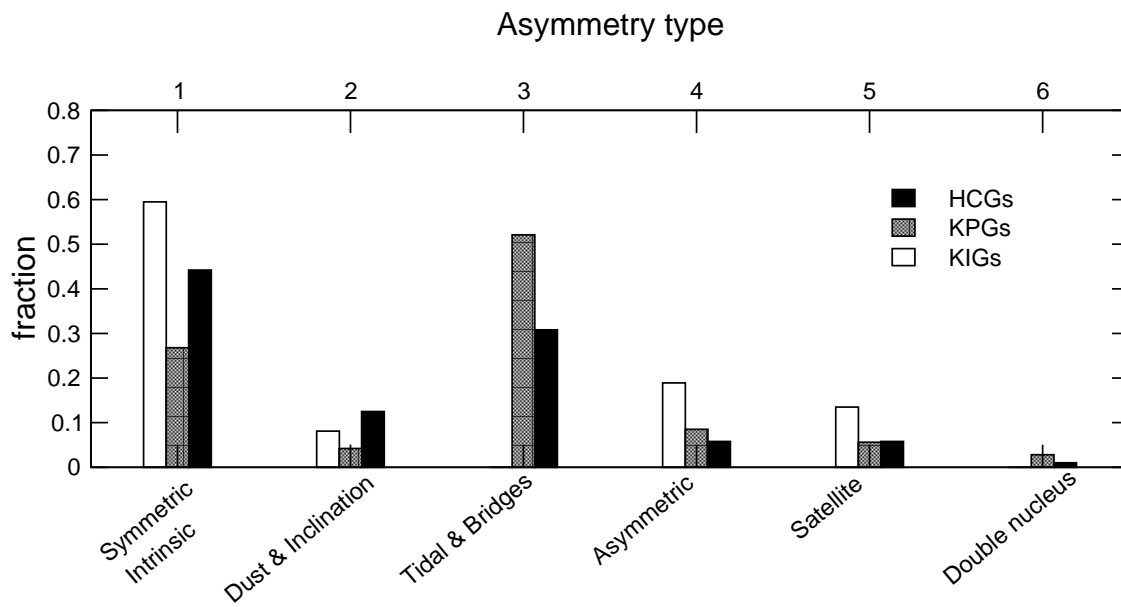


Fig. 21.— Distribution of the different asymmetry types in different environments.